

Neuronal Excitability

Activity-Dependent Inhibitory Synapse Scaling Is Determined by Gephyrin Phosphorylation and Subsequent Regulation of GABA_A Receptor Diffusion

Sereina Battaglia,⁴ Marianne Renner,^{1,2,3} Marion Russeau,^{1,2,3} Etienne Côme,^{1,2,3} Shiva K. Tyagarajan,^{4,5,*} and Sabine Lévi^{1,2,3,*}

DOI: <http://dx.doi.org/10.1523/ENEURO.0203-17.2017>

¹INSERM UMR-S, Paris, 75005, France, ²Université Pierre et Marie Curie, Paris, 75005, France, ³Institut du Fer à Moulin, Paris, 75005, France, ⁴Institute of Pharmacology and Toxicology, University of Zürich, Zurich, 8057, Switzerland, and ⁵Center for Neuroscience Zurich, Zurich, 8057, Switzerland

Abstract

Synaptic plasticity relies on the rapid changes in neurotransmitter receptor number at postsynaptic sites. Using superresolution photoactivatable localization microscopy imaging and quantum dot–based single-particle tracking in rat hippocampal cultured neurons, we investigated whether the phosphorylation status of the main scaffolding protein gephyrin influenced the organization of the gephyrin scaffold and GABA_A receptor (GABA_AR) membrane dynamics. We found that gephyrin phosphorylation regulates gephyrin microdomain compaction. Extracellular signal–regulated kinase 1/2 and glycogen synthase kinase 3β (GSK3β) signaling alter the gephyrin scaffold mesh differentially. Differences in scaffold organization similarly affected the diffusion of synaptic GABA_ARs, suggesting reduced gephyrin receptor–binding properties. In the context of synaptic scaling, our results identify a novel role of the GSK3β signaling pathway in the activity-dependent regulation of extrasynaptic receptor surface trafficking and GSK3β, protein kinase A, and calcium/calmodulin-dependent protein kinase IIα pathways in facilitating adaptations of synaptic receptors.

Key words: GABA_A receptor; homeostatic plasticity; PALM; post-translation modification; single particle tracking

Significance Statement

Our data identify phosphorylation as a key mechanism controlling the gephyrin scaffold mesh, and hence, the diffusion capture of GABA_A receptors at inhibitory synapses. We further show how critical this mechanism is for inhibitory synaptic scaling.

Introduction

Fast synaptic inhibition mediated by GABA_A receptors (GABA_ARs) plays an essential role in information transfer

between neurons. In recent years GABAergic inhibition has been shown to be dynamic, allowing flexible adaptations (Chen et al., 2012). Within the paradigm of *in vitro*

Received June 9, 2017; accepted December 21, 2017; First published January 11, 2018.

Authors report no conflict of interest.

Author contributions: SL and SKT conceptualized the project and designed the experiments. SL supervised the experimental work. SB, EC, and MRu performed immunofluorescence and SPT experiments and analyzed the data together with SL. MRu prepared primary hippocampal neurons. MRu performed the superresolution experiments, developed data analysis tools, and analyzed the data. SL and SKT wrote the manuscript.

This work was supported in part by INSERM, Sorbonne Université-UPMC, LabEx Biopsy to SL, Olgamyenfisch Grant to SKT, and University of Zurich internal funding to SKT. EC is the recipient of a doctoral fellowship from the Université Pierre et Marie Curie. STORM/PALM equipment at the IFM was supported by DIM NeRF from Région Ile-de-France and by the FRC/Rotary 'Espoir en tête.' The Lévi lab is affiliated with the Paris School of Neuroscience (ENP) and the Bio-Psy Laboratory of Excellence.

*S.K.T. and S.L. are co-senior authors.

synaptic scaling, wherein the neuronal activity is pharmacologically manipulated for several hours to days, the effects of chronic changes in activity are still poorly understood at inhibitory synapses.

Neuronal inhibition is dynamically regulated by the amount of network activity. GABA_AR stability at synaptic sites and subsequent proteasomal degradation is an essential component of synaptic homeostasis that strongly influences amplitude and frequency of miniature inhibitory postsynaptic currents (mIPSCs; Saliba et al., 2007). Similarly, lasting depolarization decreases GABA_AR internalization on principal neurons and increases GAD65 cluster size at presynaptic GABAergic terminals (Rannals and Kapur, 2011). These observations highlight that multiple systems and pathways facilitate inhibitory synapse adjustments in response to chronic changes in activity.

At postsynaptic sites, lateral diffusion in and out of synapses can also rapidly alter receptor availability on acute activity elevation (Bannai et al., 2009, 2015). Chemical-induced long-term potentiation (iLTP) enhances phosphorylation of the GABA_AR $\beta 3$ subunit at serine 383 (S383) by calcium/calmodulin-dependent protein kinase II α (CaMKII α), resulting in reduced surface mobility of GABA_ARs, synaptic enrichment of receptors, and increased inhibitory neurotransmission (Petri et al., 2014). Hence, apart from endocytosis and exocytosis, lateral diffusion of receptors could also be an effective mechanism of synaptic plasticity.

In recent years, it has become evident that the main scaffolding protein at the GABAergic synapse, gephyrin, is dynamically regulated, and this contributes to input-specific adaptations at postsynaptic sites (Chen et al., 2012; van Versendaal et al., 2012; Villa et al., 2016). Identification of signaling pathways that converge onto gephyrin scaffolds by causing posttranslational modifications of specific residues has shed new light on the molecular mechanisms underlying GABAergic synaptic plasticity. It was revealed that gephyrin phosphorylation by extracellular signal-regulated kinase 1/2 (ERK1/2) at serine 268 (S268) reduces scaffold size and GABAergic mIPSC amplitude (Tyagarajan et al., 2013). Similarly, blocking glycogen synthase kinase 3 β (GSK3 β) phosphorylation of gephyrin at serine 270 via the transgenic expression of the phospho-null mutant (S270A) significantly increases mIPSC frequency and amplitude (Tyagarajan et al., 2011). Theta burst stimulation (TBS) of CA3 Schaffer collaterals has been reported to induce gephyrin-mediated remodeling of GABAergic synapses in CA1 py-

ramidal cells (Flores et al., 2015). Although gephyrin phosphorylation at CaMKII α sites is involved in this form of structural plasticity (Flores et al., 2015), the molecular basis for gephyrin phosphorylation-induced GABA_AR synapse dynamics remains to be further explored.

To address this, we rendered gephyrin insensitive to ERK1/2 and GSK3 β signaling pathways and studied their influence on GABA_AR membrane diffusion properties. We report structural organization differences within gephyrin scaffolds based on phosphorylation status. Furthermore, cooperation between gephyrin and GABA_ARs is differentially regulated by gephyrin phosphorylation status and changes in activity.

Material and Methods

Neuronal culture

Primary cultures of hippocampal neurons were prepared from hippocampi dissected at embryonic day 18 or 19 from Sprague-Dawley rats of either sex. Tissue was trypsinized (0.25% vol/vol) and mechanically dissociated in 1 \times HBSS (Invitrogen) containing 10 mM HEPES (Invitrogen). Neurons were plated at a density of 120 \times 10³ cells/ml onto 18-mm-diameter glass coverslips (Assistant) precoated with 50 μ g/ml poly-D,L-ornithine (Sigma-Aldrich) in plating medium composed of minimum essential medium (MEM, Sigma-Aldrich) supplemented with horse serum (10% vol/vol, Invitrogen), L-glutamine (2 mM), and Na⁺ pyruvate (1 mM; Invitrogen). After attachment for 3–4 h, cells were incubated in culture medium that consists of Neurobasal medium supplemented with B27 (1 \times), L-glutamine (2 mM), and antibiotics (penicillin 200 units/ml, streptomycin, 200 μ g/ml; Invitrogen) for up to 4 wk at 37°C in a 5% CO₂ humidified incubator. Each week, one-fifth of the culture medium volume was replaced.

DNA constructs

The following constructs were used: *GEPHN* 3'-UTR shRNA and control shRNA-3m (Yu et al., 2007), DsRed-homer1c (Bats et al., 2007; provided by D. Choquet, IIN, Bordeaux, France), eGFP-gephyrin P1 variant (Lardi-Studler et al., 2007). eGFP- or pDendra2-WT, -S268E, -S270A, -DN, -S303A/S305A (SSA), and -SSA/S270A point mutants were generated using the eGFP-gephyrin P1 variant as template for site-directed mutagenesis (Tyagarajan et al., 2011, 2013; Flores et al., 2015).

Neuronal transfection

Transfections were conducted at 14–15 days *in vitro* (DIV) using Lipofectamine 2000 (Invitrogen) or Transfectin (Bio-Rad), according to the manufacturers' instructions (DNA:transfectin ratio 1 μ g:3 μ l), with 1–1.2 μ g of plasmid DNA per 20-mm well. The following ratio of plasmid DNA was used in cotransfection experiments: 0.5:0.5:0.3 μ g for eGFP-S268E/eGFP-S270A/eGFP-DN/eGFP-SSA/eGFP-SSA/S270A:*GEPHN* 3' UTR shRNA/*GEPHN* 3' UTR-3m shRNA:DsRed-homer1c. Experiments were performed 6–9 d after transfection.

Pharmacology

4-Aminopyridine (4-AP, 100 mM, Sigma-Aldrich) was directly added to the culture medium, and the neurons

Acknowledgments: We are grateful to the Cell and Tissue Imaging Facility of Institut du Fer à Moulin (IFM).

Correspondence should be addressed to either of the following: Sabine Lévi, INSERM-UPMC UMR-S 839, 17 rue du Fer à Moulin, 75005 Paris, France. E-mail: sabine.levi@inserm.fr; or Shiva Tyagarajan, Institute of Pharmacology and Toxicology, University of Zürich, Winterthurerstrasse 190, 8057 Zurich, CH, Switzerland. E-mail: tyagarajan@pharma.uzh.ch.

DOI: <http://dx.doi.org/10.1523/ENEURO.0203-17.2017>

Copyright © 2018 Battaglia et al.

This is an open-access article distributed under the terms of the Creative Commons Attribution 4.0 International license, which permits unrestricted use, distribution and reproduction in any medium provided that the original work is properly attributed.

were returned to a 5% CO₂ humidified incubator for 8 or 48 h before use. For SPT experiments, neurons were labeled at 37°C in imaging medium (see below for composition) in the presence of 4-AP, transferred to a recording chamber, and recorded within 45 min at 31°C in imaging medium in the presence of 4-AP. The imaging medium consisted of phenol red-free MEM supplemented with glucose (33 mM; Sigma-Aldrich) and Hepes (20 mM), glutamine (2 mM), Na⁺-pyruvate (1 mM), and B27 (1×) from Invitrogen.

Immunocytochemistry

Cells were fixed for 15 min at room temperature (RT) in paraformaldehyde (PFA, 4% wt/vol, Sigma-Aldrich) and sucrose (14% wt/vol, Sigma) solution prepared in PBS (1×). After washes in PBS, cells were permeabilized with Triton (0.25% vol/vol, Sigma-Aldrich) diluted in PBS. Cells were washed again in PBS and incubated for 1 h at RT in Triton (0.1% vol/vol, Sigma-Aldrich) and goat serum (GS, 10% vol/vol, Invitrogen) in PBS to block nonspecific staining. Subsequently, neurons were incubated for 1 h with a primary antibody mix consisting of guinea pig antibodies against GABA_AR α2 subunit (1:2000, provided by J.M. Fritschy, University of Zurich) and rabbit anti-VGAT (1:400, provided by B. Gasnier, University Paris Descartes, Paris) in PBS supplemented with GS (10% vol/vol, Invitrogen) and Triton (0.1% vol/vol, Sigma-Aldrich). After washes, cells were incubated for 60 min at RT with a secondary antibody mix containing biotinylated F(ab')₂ anti-guinea pig (1:300, Jackson ImmunoResearch) and AMCA350-conjugated goat anti-rabbit (1:100, Jackson Laboratory) in PBS-GS-Triton blocking solution, washed, incubated for another 45 min with streptavidin-CY5 (1:300, Thermo Fisher Scientific), and finally mounted on glass slides using Mowiol 4-88 (48 mg/ml, Sigma-Aldrich). Sets of neurons compared for quantification were labeled simultaneously.

Fluorescence image acquisition and analysis

Image acquisition was performed using a 63× objective (NA 1.32) on a Leica DM6000 upright epifluorescence microscope with a 12-bit cooled CCD camera (Micromax, Roper Scientific) run by MetaMorph software (Roper Scientific). Quantification was performed using MetaMorph software. Image exposure time was determined on bright cells to obtain the best fluorescence-to-noise ratio and avoid pixel saturation. All images from a given culture were then acquired with the same exposure time and acquisition parameters. For each image, several dendritic regions of interest were manually chosen, and a user-defined intensity threshold was applied to select clusters and avoid their coalescence. For quantification of gephyrin or GABA_AR α2 synaptic clusters, gephyrin or receptor clusters comprising at least 3 pixels and colocalized on at least 1 pixel with VGAT clusters were considered. The integrated fluorescence intensities of clusters were measured.

Live-cell staining for single-particle imaging

Neurons were incubated for 3–5 min at 37°C with primary antibodies against extracellular epitopes of GABA_AR

α2 subunit (guinea pig, 1:750/1:1000, provided by J.M. Fritschy), washed, and incubated for 3–5 min at 37°C with biotinylated Fab secondary antibodies (goat anti-guinea pig, 4–12 μg/ml; Jackson ImmunoResearch) in imaging medium. After washes, cells were incubated for 1 min with streptavidin-coated quantum dots (QDs) emitting at 605 nm (1 nM; Invitrogen) in borate buffer (50 mM) supplemented with sucrose (200 mM) or in PBS (1 M; Invitrogen) supplemented with 10% casein (vol/vol; Sigma-Aldrich). Washing and incubation steps were all done in imaging medium. To assess the membrane dynamics of GABA_AR α2 subunit at inhibitory synapses in neurons expressing the eGFP-DN mutant, inhibitory synapses were stained by incubating live neurons for 48 h at 37°C in a 5% CO₂ humidified incubator with a primary VGAT antibody directly coupled to Oyster550 (1:200, Synaptic Systems) diluted in conditioned maintenance medium.

Single-particle tracking and analysis

Cells were imaged using an Olympus IX71 inverted microscope equipped with a 60× objective (NA 1.42; Olympus) and a Lambda DG-4 monochromator (Sutter Instrument). Individual images of gephyrin-eGFP and homer1c-GFP, and QD real time recordings (integration time of 75 ms over 600 consecutive frames) were acquired with Hamamatsu ImagEM EMCCD camera and MetaView software (Meta Imaging 7.7). Cells were imaged within 45 min after labeling.

QD tracking and trajectory reconstruction were performed with Matlab software (The Mathworks). One to two subregions of dendrites were quantified per cell. In cases of QD crossing, the trajectories were discarded from analysis. Trajectories were considered synaptic when overlapping with the synaptic mask of gephyrin-eGFP or VGAT-Oyster550 clusters, or extrasynaptic for spots 2 pixels (380 nm) away (Lévi et al., 2008). Values of the mean square displacement (MSD) plot versus time were calculated for each trajectory by applying the relation

$$MSD(n\tau) = \frac{1}{N - n} \sum_{i=1}^{N-n} (\{x[(i + n)\tau] - x(i\tau)\}^2 + \{y[(i + n)\tau] - y(i\tau)\}^2),$$

(Saxton and Jacobson, 1997), where τ is the acquisition time, N is the total number of frames, and n and i are positive integers with n determining the time increment. Diffusion coefficients (D) were calculated by fitting the first four points without origin of the MSD versus time curves with the equation: $MSD(n\tau) = 4Dn\tau + b$, where b is a constant reflecting the spot localization accuracy. Synaptic dwell time was defined as the duration of detection of QDs at synapses on a recording divided by the number of exits as detailed previously (Ehrensperger et al., 2007; Charrier et al., 2010). Dwell times ≤ 5 frames were not retained. The explored area of each trajectory was defined as the MSD value of the trajectory at two different time intervals of 0.42 and 0.45 s (Renner et al., 2012).

PALM imaging

Photoactivatable localization microscopy (PALM) imaging on fixed samples was conducted on an inverted N-STORM Nikon Eclipse Ti microscope with a 100 \times oil-immersion objective (NA 1.49) and an Andor iXon Ultra EMCCD camera (image pixel size, 160 nm), using specific lasers for PALM imaging of Dendra2 (405 and 561 nm). Videos of 10,000 frames were acquired at frame rates of 50 ms. The z position was maintained during acquisition by a Nikon perfect focus system. Single-molecule localization and 2D image reconstruction was conducted as described in Specht et al. (2013) by fitting the PSF of spatially separated fluorophores to a 2D Gaussian distribution. The position of fluorophore were corrected by the relative movement of the synaptic cluster by calculating the center of mass of the cluster throughout the acquisition using a partial reconstruction of 2000 frames with a sliding window (Specht et al., 2013). PALM images were rendered by superimposing the coordinates of single-molecule detections, which were represented with 2D Gaussian curves of unitary intensity and SDs representing the localization accuracy ($\sigma = 20$ nm). To correct multiple detections coming from the same pDendra2 molecule (Specht et al., 2013), we identified detections occurring in the vicinity of space ($2 \times \sigma$) and time (15 s) as belonging to the same molecule. The surface of gephyrin clusters and the densities of gephyrin molecules per square micrometer were measured in reconstructed 2D images through cluster segmentation based on detection densities. The threshold to define the border was set to 1000 detections/ μm^2 , taking into account the reported gephyrin densities in synapses (Specht et al., 2013; Fig. 3B). Briefly, all pixels (PALM pixel size = 20 nm) containing <2 detections were considered empty, and their intensity value was set to 0. The intensity of pixels with ≥ 2 detections was set to 1. The resulting binary image was analyzed with the function “regionprops” of Matlab to extract the surface area of each cluster identified by this function. Density was calculated as the total number of detections in the pixels belonging to a given cluster, divided by the area of the cluster.

Statistics

Sampling corresponds to the number of quantum dots for SPT, the number of cells for ICC, and the number of synapses for PALM. Sample size selection for experiments was based on published experiments, pilot studies, and in-house expertise. All results were used for analysis except in a few cases. Cells with signs of suffering (apparition of blobs, fragmented neurites) were discarded from the analysis. Means \pm SEM are shown, and median values are indicated with their interquartile range (IQR, 25%–75%). Means were compared using the nonparametric Mann–Whitney test (immunocytochemistry, dwell time comparison, PALM quantifications) using SigmaPlot 12.5 (Systat Software). For diffusion coefficient and explored area values having nonnormal distributions, a nonparametric Kolmogorov–Smirnov test was run in Matlab. Differences were considered significant for p -values $<5\%$.

Results

eGFP-gephyrin mutants exhibit different clustering properties in culture

Signaling pathways that converge onto gephyrin scaffolding properties influence GABA_AR synaptic transmission. Hence, mimicking phosphorylation/dephosphorylation events that influence gephyrin clustering can help gain critical insights into nanoscale regulation of GABA_ARs at synaptic sites. ERK1/2 phosphorylation at the S268 residue results in smaller gephyrin clusters (Tyagarajan et al., 2013); hence, we selected phosphomimetic eGFP-gephyrin-S268E mutant to study the impact of smaller clusters on receptor diffusion. Similarly, pharmacological blockade of the GSK3 β pathway or eGFP-gephyrin-S270A mutant expression increases gephyrin cluster number and size (Tyagarajan et al., 2011). We selected the eGFP-S270A mutant to understand how larger clusters would impact receptor diffusion. eGFP-gephyrin dominant negative (DN) mutant in primary neurons not only abolishes gephyrin clustering and reduces surface expression of GABA_ARs, but also significantly decreases GABAergic mIPSC amplitude and frequency (Ghosh et al., 2016). Hence, we selected eGFP-DN mutant to evaluate how cluster disruption would impact synaptic anchoring and surface diffusion of GABA_ARs.

Primary hippocampal neurons were cotransfected at 14 DIV with eGFP-gephyrin WT (eGFP-WT), eGFP-S268E, eGFP-S270A, or eGFP-DN along with shRNA targeting the gephyrin 3' UTR (to minimize the influence of endogenous gephyrin expression on mutant phenotypes). Before studying the influence of altered gephyrin clustering on GABA_AR diffusion properties, we confirmed the respective gephyrin mutant morphology 6–9 d after transfection. Representative images of neurons expressing either eGFP-WT or eGFP-S268E, eGFP-S270A, eGFP-DN variants are shown (Fig. 1A). We stained for the $\alpha 2$ GABA_AR subunit to study the relation of eGFP-gephyrin with receptors. Quantification for eGFP-gephyrin cluster density (N_b), cluster size (area), and intensity (Int) showed a tendency for reduced clustering for the S268E mutant and increased clustering for the S270A mutant (Fig. 1B). The impact of the gephyrin S270A mutation on gephyrin cluster area and intensity was more pronounced, in comparison to the S268E mutant. As expected, eGFP-DN failed to cluster (data not shown). Similar to the observed changes in eGFP-gephyrin morphology, quantification of cluster intensity for $\alpha 2$ GABA_AR showed a significant increase in neurons expressing eGFP-S270A, whereas eGFP-S268E expressing neurons showed only a modest reduction in $\alpha 2$ (Fig. 1C). The neurons expressing eGFP-DN showed very little $\alpha 2$ GABA_AR staining (data not shown).

Influence of eGFP-gephyrin mutants on GABA_AR surface diffusion

GABA_ARs are known to exhibit faster mobility at extrasynaptic sites compared with synaptic sites. Because of their interaction with the main scaffolding molecule gephyrin, GABA_ARs are slowed down and confined at synapses. This diffusion-capture of GABA_ARs is modu-

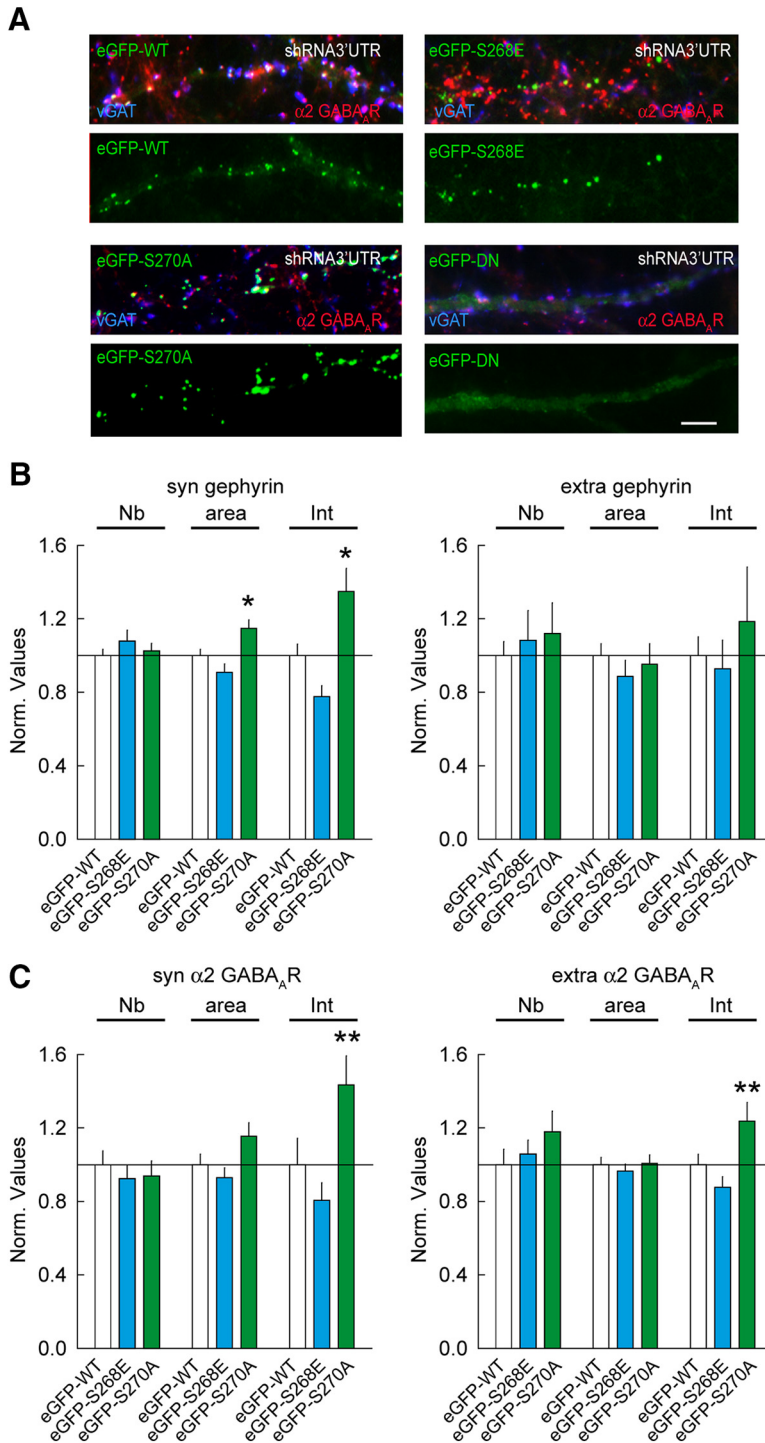


Figure 1. Morphologic characterization of eGFP-gephyrin and its mutant variants. **A**, Representative images of primary hippocampal neurons cotransfected with eGFP-WT, eGFP-S268E, eGFP-S270A, or eGFP-DN and shRNA-3' UTR. eGFP-gephyrin clusters (green), $\alpha 2$ GABA_ARs (red), and VGAT (blue) are shown. Scale bar, 10 μ m. **B**, Quantification of eGFP-gephyrin cluster density, cluster area, and intensity shows larger eGFP-S270A clusters compared with eGFP-WT at synapses. S268E: WT $n = 66$ cells, S268E $n = 60$ cells, 4 cultures. Syn: Cluster Number (Nb) $p = 0.42$, area $p = 0.22$, intensity $p = 0.05$. Extra: Nb $p = 0.99$, Area $p = 0.66$, Intensity $p = 0.44$. S270A: WT $n = 86$ cells, S270A: $n = 74$ cells, 6 cultures. Syn: Nb $p = 0.77$, Area $p = 0.02$, Intensity $p = 0.02$. Extra: Nb $p = 0.39$, Area $p = 0.42$, Intensity $p = 0.15$. **C**, Quantification for $\alpha 2$ GABA_AR clusters shows significantly more receptors in eGFP-S270A mutant clusters. S268E: WT $n = 52$ cells, S268E $n = 47$ cells, 3 cultures. Syn: Nb $p = 0.48$, Area $p = 0.46$, Intensity $p = 0.6$. Extra: Nb $p = 0.46$, area $p = 0.63$, intensity $p = 0.22$. S270A: WT $n = 52$ cells, S270A $n = 39$ cells, 3 cultures. Syn: Nb $p = 0.56$, Area $p = 0.08$, Intensity $p = 0.008$. Extra: Nb $p = 0.008$, Area $p = 0.81$, Intensity $p = 0.29$. Data shown as mean \pm SEM. Values were normalized to the corresponding control values. Statistics *, $p \leq 0.05$, **, $p \leq 0.01$ (Mann-Whitney rank sum test).

lated by neuronal activity and constitutes an important basis for synaptic plasticity (Petrini and Barberis, 2014). The expression of specific eGFP-gephyrin mutations allows us to lock the scaffold into different conformations and study its influence on GABA_AR surface diffusion. To achieve this, we assessed the lateral mobility of $\alpha 2$ GABA_AR using quantum dot–based single-particle tracking (QD-SPT). Live imaging over 600 constitutive frames at 75 Hz was used to record individual trajectories, and the trajectories were later analyzed using custom software (Fig. 2A; see Methods). As a proof of concept, we first tested the effect of total gephyrin cluster removal on $\alpha 2$ GABA_AR surface dynamics by expressing the eGFP-DN mutant. However, given that eGFP-DN has a diffuse expression, to distinguish synaptic and extrasynaptic $\alpha 2$ clusters we preloaded presynaptic GABAergic terminals using VGAT-Oyster550 antibody. The expression of the eGFP-DN mutant increased the surface exploration of QDs at both extrasynaptic and synaptic sites compared with control eGFP-WT. Quantification of the $\alpha 2$ GABA_AR diffusion coefficient showed a 1.4-fold increase for extrasynaptic receptors and a 1.2-fold increase for synaptic receptors in eGFP-DN–expressing neurons (Fig. 2B). Areas explored by $\alpha 2$ GABA_AR also showed a 1.6-fold increase at extrasynaptic sites and a 1.3-fold increase at synaptic sites in eGFP-DN–expressing neurons (Fig. 2C). These observations support the notion that gephyrin slows down and confines GABA_AR not only at synapses but also at extrasynaptic sites (Ehrensperger et al., 2007).

Synaptic dwell time values can be discriminated from “trapped” receptors (dwell time >5.9 s) and “passing” receptors (dwell time ≤ 5.9 s; Renner et al., 2012). Quantification of $\alpha 2$ GABA_AR dwell time confirmed a 1.3-fold faster escape time of receptors in neurons expressing the eGFP-DN mutant (Fig. 2D). We did not observe any difference in this rate for passing receptors. This is an indication that the observed reduction of trapped receptors is not due to increased membrane viscosity, but rather to gephyrin scaffold’s influence on GABA_AR surface mobility. Thus, we concluded that the diffuse DN gephyrin relieved GABA_AR $\alpha 2$ diffusion constraints, leading to synaptic escape of receptors.

If gephyrin clustering can indeed influence receptor diffusion, then S268E and S270A modifications must have an influence on $\alpha 2$ GABA_AR surface mobility. To test this, we transfected the eGFP-S268E or eGFP-S270A mutants and measured surface mobility at extrasynaptic and synaptic locations. Superimposition of trajectories with fluorescent images of eGFP-gephyrin allowed us to distinguish synaptic versus extrasynaptic $\alpha 2$ GABA_AR. Neurons transfected with eGFP-S268E exhibited an increase in surface exploration of individual trajectories (Fig. 2A). This was consistent with the observed increase in diffusion coefficients at both extrasynaptic and synaptic sites (Fig. 2E). Similarly, quantification of explored areas at both extrasynaptic and synaptic sites showed significant increases (Fig. 2F). If reducing gephyrin cluster size facilitates $\alpha 2$ diffusion, then we would expect shorter dwell time at synaptic sites. Indeed, we report reduced dwell time for trapped $\alpha 2$ GABA_AR in eGFP-S268E–trans-

ected neurons (Fig. 2G). Therefore the use of eGFP-S268E gephyrin mutant shows that the reduction in gephyrin cluster size causes an increase in GABA_AR diffusion, while reducing synaptic dwell time.

On the other hand, in eGFP-S270A–transfected neurons, the $\alpha 2$ GABA_AR showed increased surface exploration of individual trajectories at synapses (Fig. 2A). Unexpectedly, diffusion coefficients and surface exploration of $\alpha 2$ extrasynaptic and synaptic GABA_AR were significantly increased in eGFP-S270A–transfected neurons (Fig. 2E,F). However, analysis showed no reduction in $\alpha 2$ GABA_AR dwell time at synaptic sites (Fig. 2G). We thus concluded that the increase in receptor mobility at synapses in S270A–transfected neurons does not correlate with what we may expect from a larger scaffold, suggesting additional regulations are at play.

Superresolution PALM microscopy reveals differential packing of gephyrin scaffold

We turned to quantitative nanoscopic imaging to understand the influence of phosphorylation on gephyrin scaffold organization. Using photoactivated localization microscopy (PALM), we estimated localization accuracy from several detections of the same fluorophore from subsequent image frames (Specht et al., 2013). The spatial resolution of PALM is within the range of ~ 25 – 30 nm; hence, image segmentation of the rendered PALM images can resolve substructure organization within a gephyrin cluster that are not discernable using diffraction-limited imaging (Specht et al., 2013).

Employing fluorescence imaging on primary hippocampal neurons cotransfected with photoconvertible pDendra2-WT, pDendra2-S268E, or pDendra2-S270A and shRNA 3’ UTR showed a clustering phenotype consistent with eGFP-gephyrin and its mutant variants (Fig. 3A). PALM image cluster segmentation was established based on local density of detections using a threshold of 1000 detections/ μm^2 (Fig. 3B). Image segmentation allows us to estimate the mean surface area of a given pDendra2-WT cluster. In this case, quantification showed pDendra2-WT clusters to be $0.054 \pm 0.003 \mu\text{m}^2$, corresponding to the mean diameter of 262 nm as has been reported earlier (Specht et al., 2013). pDendra2-S268E quantifications showed a significant reduction in mean surface area to $0.035 \pm 0.002 \mu\text{m}^2$, and consistent with our expectations, pDendra2-S270A showed an increase in cluster area of $0.078 \pm 0.005 \mu\text{m}^2$ (Fig. 3C).

We next tried to correlate the estimated size of gephyrin clusters to their respective densities. Our analysis showed 3919.7 ± 227.9 molecules/ μm^2 of pDendra2-WT within a cluster (Fig. 3D). pDendra2-S268E showed a significantly increased molecular density (4457.5 ± 221.6) despite having a smaller cluster area. In contrast, pDendra2-S270A mutant shows a significantly reduced molecular density (2819.8 ± 117.6), despite having a larger surface area (Fig. 3D).

Our data indicate that there is no correlation between the diffusion properties of GABA_AR despite the relative size difference between S268E and S270A gephyrin clusters. However, there is a strong correlation between

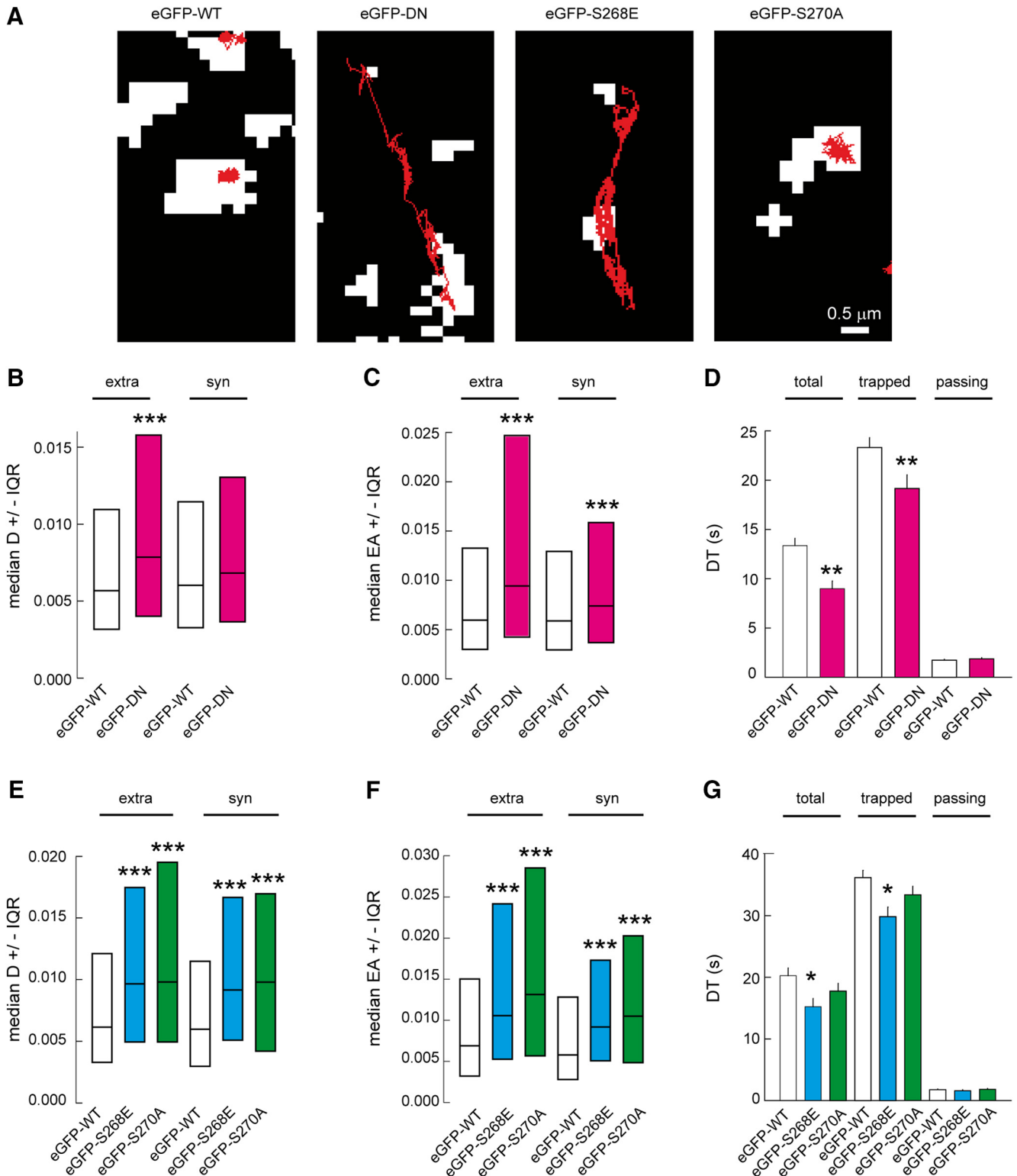


Figure 2. Membrane dynamics of $\alpha 2$ GABA_AR is influenced by gephyrin phosphorylation. **A**, Example traces of QD trajectories (red) overlaid with fluorescent synaptic clusters (white) of VGAT-Oyster550 for eGFP-DN transfected neurons or with eGFP-gephyrin clusters for eGFP-WT, eGFP-S268E, or eGFP-S270A expressing cells. Scale bar, 0.5 μ m. **B**, Median diffusion coefficients D of $\alpha 2$ GABA_AR in neurons transfected with either eGFP-WT or eGFP-DN. Extra: WT $n = 975$ QDs, DN $n = 491$ QDs, $p = 4.5 \times 10^{-34}$; Syn: WT $n = 306$ QDs, DN $n = 173$ QDs, $p = 0.36$. **C**, Quantification of explored area EA of $\alpha 2$ GABA_AR, Extra: WT $n = 2925$ QDs, DN $n = 1473$ QDs, $p = 3.8 \times 10^{-23}$; Syn: WT $n = 918$ QDs, DN $n = 519$ QDs, $p = 4.4 \times 10^{-4}$. **D**, Dwell time DT of $\alpha 2$ GABA_AR at synapses in neurons transfected with either eGFP-WT or eGFP-DN. Quantification of all QDs (total), trapped (DT < 5.9 s), and passing (DT > 5.9 s) QDs at inhibitory synapses. Significant decrease in synaptic dwell time for total and trapped QDs was observed but not for

continued

passing ones. Total: WT $n = 436$ QDs, DN $n = 262$ QDs, $p = 0.001$; Trapped: WT $n = 235$ QDs, DN $n = 108$ QDs, $p = 8.0 \times 10^{-3}$; Passing: WT $n = 201$ QDs, DN $n = 154$ QDs, $p = 0.19$. **E**, Quantification of diffusion coefficients of $\alpha 2$ GABA_AR showing increased receptor mobility at extrasynaptic (extra) and synaptic (syn) sites in neurons transfected with eGFP-S268E or eGFP-S270A, compared with eGFP-WT expressing cells. Extra: WT $n = 1820$ QDs, S268E $n = 1273$ QDs, $p = 1.1 \times 10^{-22}$, S270A $n = 1658$, $p = 2.9 \times 10^{-27}$. Syn: WT $n = 461$ QDs, S268E $n = 326$ QDs, $p = 2.4 \times 10^{-8}$, S270A $n = 340$, $p = 1.8 \times 10^{-8}$. **F**, Quantification of $\alpha 2$ GABA_AR explored area EA, Extra: WT $n = 5460$ QDs, S268E $n = 3807$ QDs, $p = 6.8 \times 10^{-52}$, S270A $n = 5355$, $p = 2.2 \times 10^{-101}$. Syn: WT $n = 1383$ QDs, S268E $n = 978$ QDs, $p = 7.4 \times 10^{-23}$, S270A $n = 2208$, $p = 1.2 \times 10^{-33}$. **G**, Quantification of $\alpha 2$ GABA_AR dwell time DT in neurons expressing eGFP-WT, eGFP-S268E, or eGFP-S270A. Calculations were done for all QDs (total), (trapped), or (passing) QDs at inhibitory synapses. Decrease in dwell time for the whole or trapped population of QDs was seen in synapses expressing eGFP-S268E but not in synapses expressing eGFP-S270A. Total: WT $n = 251$ QDs, S268E $n = 176$ QDs, $p = 0.013$, S270A $n = 216$ QDs, $p = 0.31$; Trapped: WT $n = 135$ QDs, S268E $n = 85$ QDs, $p = 0.002$, S270A $n = 109$ QDs, $p = 0.28$; Passing: WT $n = 116$ QDs, S268E $n = 91$ QDs, $p = 0.24$, S270A $n = 107$ QDs, $p = 0.98$. All data are from six independent experiments. In **B**, **C**, **E**, and **F**, data are presented as median values \pm 25%–75% IQR, ***, $p \leq 0.001$ (Kolmogorov–Smirnov test). In **D** and **G**, data are presented as mean \pm SEM. *, $p \leq 0.05$, **, $p \leq 0.01$ (Mann–Whitney rank sum test). D in $\mu\text{m}^2/\text{s}$, EA in μm^2 , DT in s.

gephyrin phosphorylation and cluster microdomain compaction. The compaction of the scaffold or the increased spacing between gephyrin molecules may perturb the

organization of the gephyrin microdomain, thereby altering gephyrin-receptor binding properties. We cannot exclude the possibility that the mutations directly affect

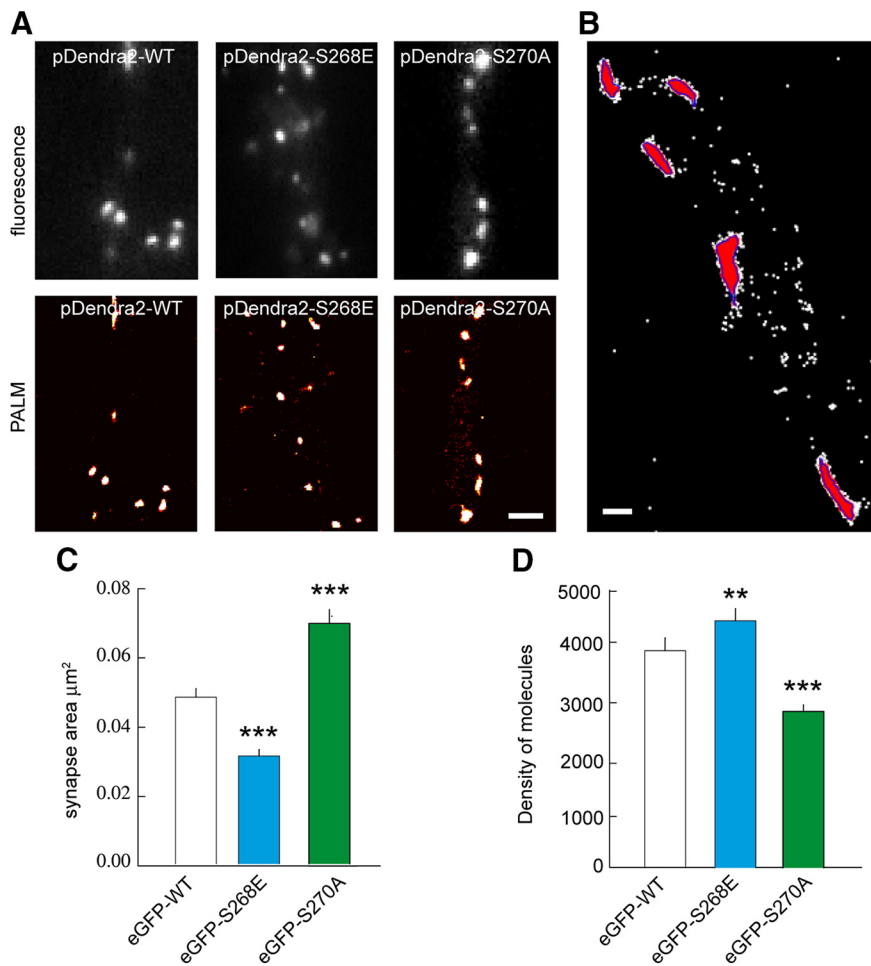


Figure 3. PALM imaging showing gephyrin phosphorylation influences scaffold packing. **A**, Epifluorescence (top) and PALM (bottom) imaging of the same dendritic regions in neurons expressing pDendra2-WT, -S268E, or -S270A mutant. Scale bar, 1 μm . **B**, Representative image of cluster segmentation (red) based on local density of molecules detected (white dots) using a threshold of 1000 detections/ μm^2 (blue). Scale bar, 200 nm. **C**, Quantification of eGFP cluster area using PALM shows reduction in cluster size for eGFP-S268E and increase in cluster size for eGFP-S270A compared with eGFP-WT. WT $n = 313$ synapses, S268E $n = 277$ synapses, S270A $n = 290$ synapses, $p < 0.001$, 4 cultures. **D**, Quantification of density of gephyrin molecules per square micrometer using PALM in transfected neurons. Neurons expressing eGFP-S268E exhibit denser gephyrin packing, and neurons expressing eGFP-S270A exhibit less dense packing of gephyrin compared with eGFP-WT. Data are presented as mean \pm SEM. **, $p = 0.006$; ***, $p \leq 0.001$ (Mann–Whitney rank sum test).

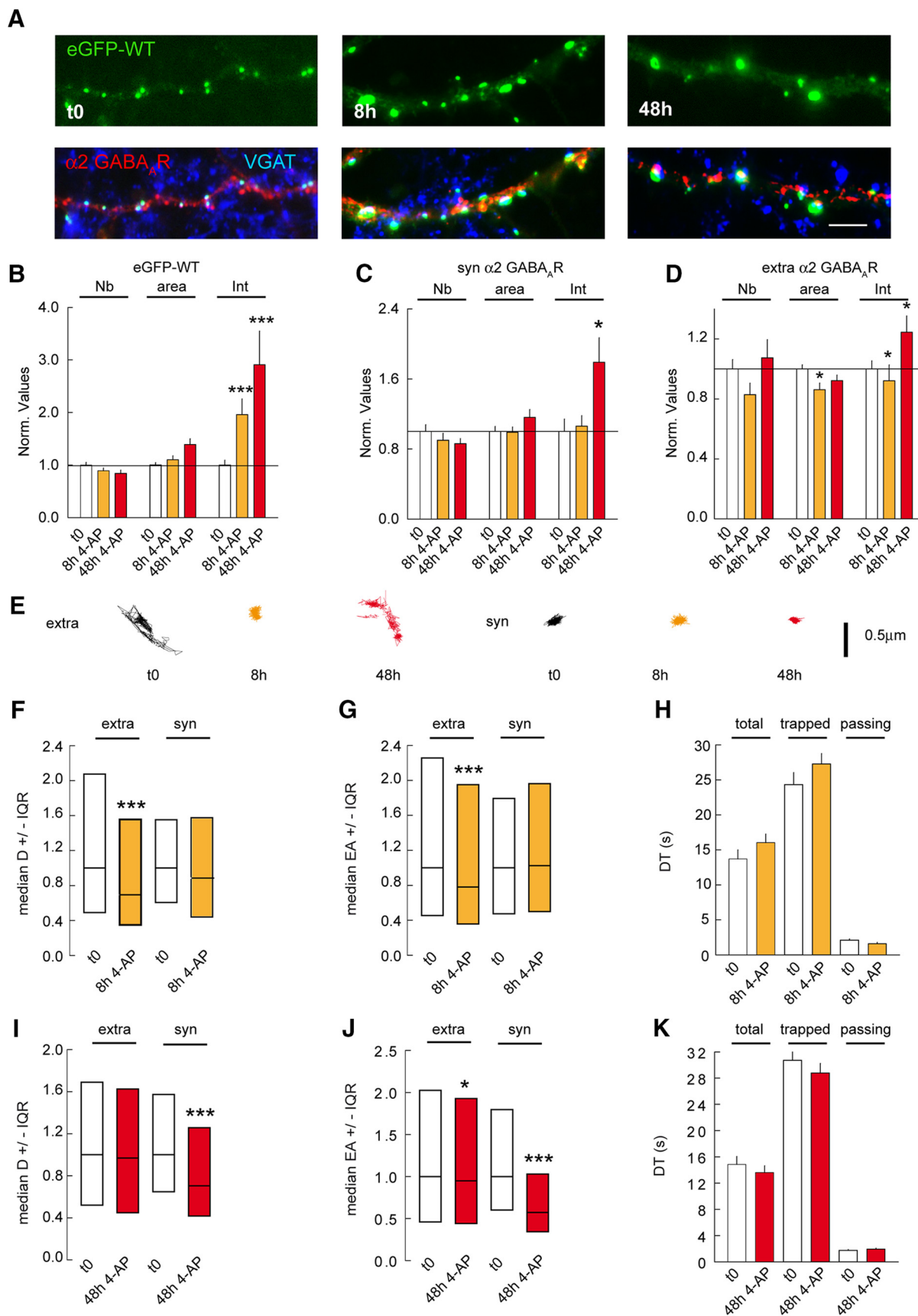


Figure 4. Gephyrin clustering influences GABA_AR lateral diffusion. **A**, Morphology of eGFP-WT (green) after 8 and 48 h of 4-AP

continued

application; VGAT (blue), GABA_AR $\alpha 2$ (red) at 21 DIV. Scale bar, 10 μm . **B**, Quantification of eGFP-WT clusters after 8 and 48 h of 4-AP application. t0 $n = 55$ cells, 8 h $n = 46$ cells, 48 h $n = 55$ cells, 3 cultures. Cluster Nb: 0–8 h: $p = 0.13$, 0–48 h: $p = 0.002$; Area: 0–8 h: $p = 0.5$, 0–48 h: $p = 0.001$; Intensity: 0–8 h: $p < 0.001$, 0–48 h: $p < 0.001$. **C**, Quantification of synaptic $\alpha 2$ GABA_AR clusters after 8 and 48 h of 4-AP compared with mock treated control. t0 $n = 52$ cells, 8 h $n = 43$ cells, 48 h $n = 53$ cells, 3 cultures. Cluster Nb: 0–8 h: $p = 0.4$, 0–48 h: $p = 0.3$; Area: 0–8 h: $p = 0.8$, 0–48 h: $p = 0.8$; Intensity: 0–8 h: $p = 0.5$, 0–48 h: $p = 0.03$. **D**, Quantification of extrasynaptic $\alpha 2$ GABA_AR clusters after 8 and 48 h of 4-AP compared with mock treated control. t0 $n = 52$ cells, 8 h $n = 43$ cells, 48 h $n = 53$ cells, 3 cultures. Cluster Nb: 0–8 h: $p = 0.2$, 0–48 h: $p = 0.9$; Area: 0–8 h: $p = 0.02$, 0–48 h: $p = 0.3$; Intensity: 0–8 h: $p = 0.05$, 0–48 h: $p = 0.022$. **E**, Example trace of $\alpha 2$ GABA_AR trajectories showing surface exploration of extrasynaptic and synaptic receptors after 8 and 48 h of 4-AP exposure. Scale bar, 0.5 μm . **F**, Quantification of diffusion coefficients of $\alpha 2$ GABA_AR after 8 h of 4-AP exposure. Extra; t0 $n = 450$ QDs, WT 4AP 8 h $n = 961$ QDs, $p = 1.96 \times 10^{-7}$. Syn; t0 $n = 103$ QDs, 8 h $n = 138$ QDs, $p = 0.22$; 2 cultures. **G**, Quantification of explored area EA of $\alpha 2$ GABA_AR after 8 h of 4-AP application. Extra; t0 $n = 1347$ QDs, 8 h $n = 5265$ QDs, $p = 6.4 \times 10^{-9}$. Syn; t0 $n = 308$ QDs, 8 h $n = 708$ QDs, $p = 0.63$. **H**, Quantification of synaptic dwell time DT of $\alpha 2$ GABA_AR showing no impact after 8 h of 4-AP for total, trapped, or passing receptor population. Total: t0 $n = 151$ QDs, 8 h $n = 206$ QDs, $p = 0.073$; Trapped: t0 $n = 80$ QDs, 8 h $n = 116$ QDs, $p = 0.36$; Passing: t0 $n = 78$ QDs, 8 h $n = 90$ QDs, $p = 0.02$. **I**, Quantification of diffusion coefficients of $\alpha 2$ GABA_AR after 48 h of 4-AP application. Extra: t0 $n = 777$ QDs, 48 h $n = 174$ QDs, $p = 0.69$. Syn: t0 $n = 126$ QDs, 48 h $n = 213$ QDs, $p = 1.4 \times 10^{-4}$. **J**, Quantification of explored area EA of $\alpha 2$ GABA_AR after 48 h of 4-AP application. Extra: t0 $n = 2331$ QDs, 48 h $n = 5508$ QDs, $p = 0.045$. Syn: t0 $n = 378$ QDs, 48 h $n = 717$ QDs, $p = 2.2 \times 10^{-20}$. **K**, Quantification of $\alpha 2$ GABA_AR dwell time after 48 h of 4-AP application. Total: t0 $n = 201$ QDs, 48 h $n = 254$ QDs, $p = 0.74$. Trapped: t0 $n = 91$ QDs, 48 h $n = 110$ QDs, $p = 0.99$. Passing: t0 $n = 110$ QDs, 48 h $n = 144$ QDs, $p = 0.81$. In **B–D**, **H**, and **K**, data are presented as mean \pm SEM, *, $p \leq 0.05$; ***, $p \leq 0.001$ (Mann–Whitney rank sum test). In **F**, **G**, **I**, and **J**, data are presented as median values \pm 25%–75% IQR, *, $p \leq 0.05$; ***, $p \leq 0.001$ (Kolmogorov–Smirnov test). In **B–G**, **I**, and **J**, values were normalized to the corresponding control values. In **H** and **K**, DT in s.

receptor-binding properties independently of their effect on the mesh.

Prolonged neuronal activity influences gephyrin and GABA_AR clustering as well as GABA_AR diffusion

Activity-dependent regulation of receptor lateral diffusion is an essential contributor to synapse adaptation (Lüscher et al., 2011). This phenomenon has been explored within the experimental paradigm of short-term (1- to 60-min) drug applications (Bannai et al., 2009, 2015; Muir et al., 2010; Niwa et al., 2012; Petrini et al., 2014). There is accumulating evidence that synaptic adaptations at GABAergic synapses also occur in response to prolonged changes in activity (Rannals and Kapur, 2011; Vlachos et al., 2013; Flores et al., 2015). Hence, we examined whether gephyrin phosphorylation regulates activity-dependent membrane diffusion and synaptic recruitment of $\alpha 2$ GABA_ARs. To test this hypothesis, we chronically elevated synaptic activity by treating our primary hippocampal neurons with the potassium channel blocker 4-aminopyridine (4-AP; 100 μM ; Chamma et al., 2013) for 8 or 48 h. We used immunocytochemistry to determine the impact of a prolonged activity increase on gephyrin and $\alpha 2$ GABA_AR clustering (Fig. 4A). Quantification across independent experiments showed that fluorescence intensity of eGFP-WT gephyrin clusters increased by 1.95-fold after 8 h and 2.3-fold after 48 h of 4-AP treatment (Fig. 4B). Quantification for $\alpha 2$ GABA_AR cluster intensity after 8 h of 4-AP-induced neuronal activity did not show an increase in receptor accumulation at synapses; however, after 48 h of 4-AP treatment, we found a 1.7-fold increase in receptor density at synaptic sites (Fig. 4C). Thus, gephyrin recruitment at synapses precedes that of the receptor in response to chronic changes in activity. In contrast to synaptic clusters, extrasynaptic $\alpha 2$ clusters decreased in size and intensity after 8 h of 4-AP application (Fig. 4D). This transient

decrease in extrasynaptic $\alpha 2$ clusters intensity is reversed after 48 h of 4-AP, similar to synaptic receptor clusters (Fig. 4C,D). Therefore, a chronic increase in activity regulates both extrasynaptic and synaptic receptor clustering.

It has been reported that acute 4-AP treatment increases GABA_AR mobility between synaptic and extrasynaptic sites (Bannai et al., 2009). Hence, we analyzed $\alpha 2$ GABA_AR surface diffusion at extrasynaptic and synaptic sites after either 8 or 48 h of 4-AP treatment using QD-SPT (Fig. 4E). Quantification of the receptor diffusion coefficient showed a 1.3-fold reduction for extrasynaptic receptors; however, the synaptic receptors were not influenced by 8 h of 4-AP treatment (Fig. 4F). Consistently, 8 h of 4-AP treatment reduced the explored area for only the extrasynaptic receptors by 1.2-fold (Fig. 4G). The receptor dwell time at synaptic sites was also unchanged after 8 h of activity change (Fig. 4H). This is consistent with a lack of receptor accumulation at synapses after 8 h of 4-AP treatment.

Contrary to the 8-h 4-AP treatment, 48-h treatment significantly reduced the diffusion coefficients of synaptic $\alpha 2$ receptors by 1.3-fold, while having no effect on the extrasynaptic receptors (Fig. 4I). We also observed a 1.3-fold reduction in explored area for synaptic $\alpha 2$ GABA_ARs, with only a modest reduction for extrasynaptic receptors (Fig. 4J). Unexpectedly, the reduction in the diffusion rate and explored area of synaptic $\alpha 2$ receptors had no influence on the dwell time at synaptic sites (Fig. 4K). Therefore, pools of extrasynaptic and synaptic receptor are regulated independently of each other over prolonged activity change.

Altogether, our data show that GABA_AR lateral diffusion can be regulated on a time scale of days. We observe a decrease in synaptic GABA_AR diffusion at the 48-h time point and not at 8 h, which is in direct correlation to cluster intensity change observed after 48 h. Therefore, regulation of GABA_AR diffusion capture accounts for the change

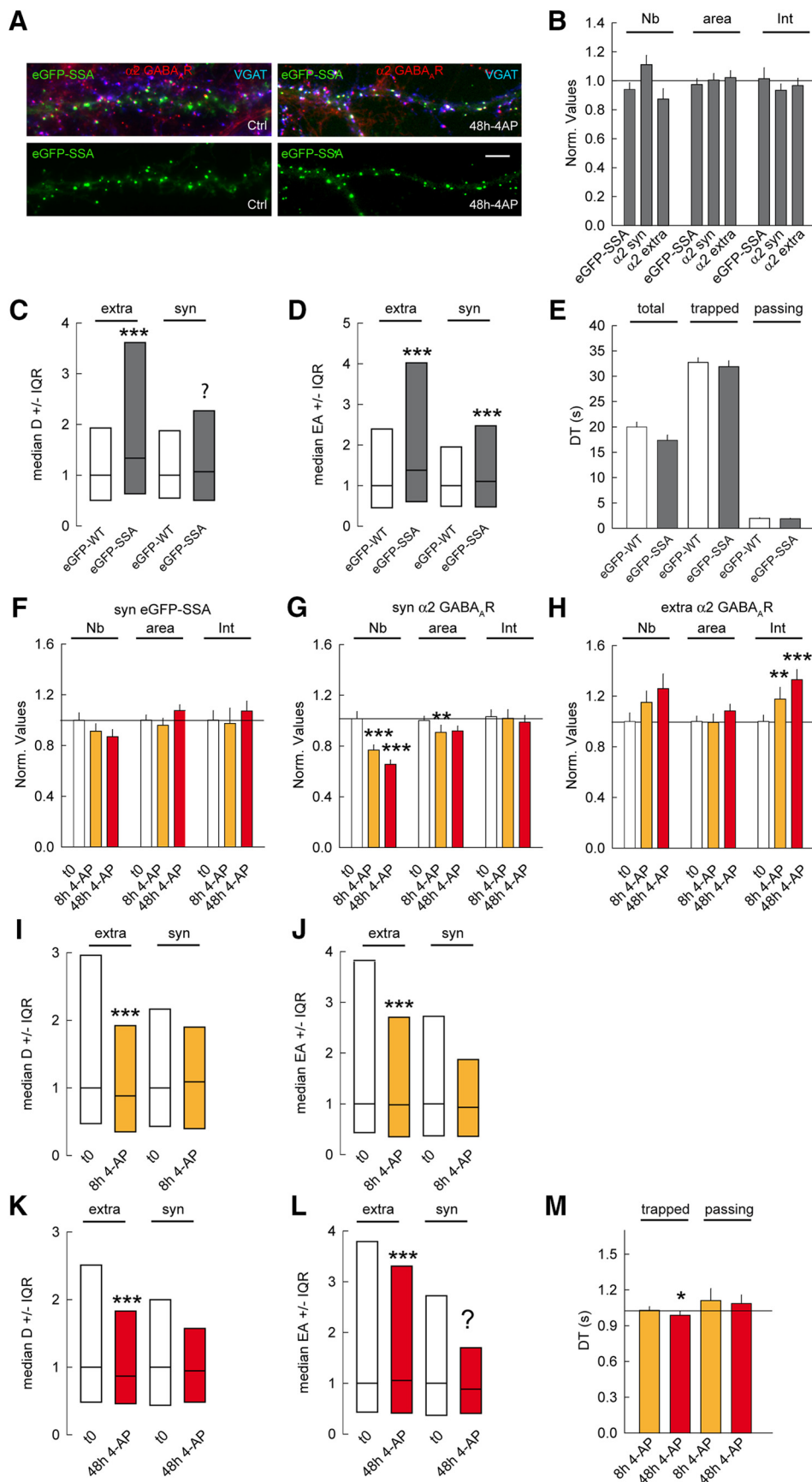


Figure 5. PKA and CaMKII α signaling pathways regulate gephyrin clustering and $\alpha 2$ GABA_AR membrane dynamics in conditions of

continued

chronic changes of activity. **A**, Morphologic analysis of neurons transfected with eGFP-S303A/S305A (eGFP-SSA) gephyrin double mutant insensitive to PKA and CaMKII α signaling pathways. Double staining of VGAT (blue) and $\alpha 2$ GABA $_A$ R (red) at 21 DIV under control condition (t0) or in the presence of 4-AP for 48 h. Scale bar, 10 μ m. **B**, Quantifications of synaptic eGFP-SSA clusters and synaptic ($\alpha 2$ syn) and extrasynaptic ($\alpha 2$ extra) $\alpha 2$ GABA $_A$ R clusters in relation to eGFP-WT show minor impact of eGFP-SSA under control condition. eGFP-WT: $n = 89$ cells, eGFP-SSA $n = 95$ cells, 6 cultures. eGFP-SSA: Cluster Nb: $p = 0.3$; Area: $p = 0.9$; Intensity: $p = 0.5$. $\alpha 2$ syn: Cluster Nb: $p = 0.4$; Area: $p = 0.5$; Intensity: $p = 0.8$. $\alpha 2$ extra: Cluster Nb: $p = 0.2$; Area: $p = 0.4$; Intensity: $p = 0.2$. **C**, Quantification of median diffusion coefficient D of $\alpha 2$ GABA $_A$ R in neurons expressing eGFP-WT or eGFP-SSA under control condition. Extra: WT $n = 1166$ QDs, SSA $n = 989$ QDs, $p = 1.5 \times 10^{-12}$; Syn: WT $n = 312$ QDs, SSA $n = 245$ QDs, $p = 0.08$; 4 cultures. **D**, Quantification of median explored area EA of $\alpha 2$ GABA $_A$ R in neurons expressing eGFP-WT or eGFP-SSA under control condition. Extra: WT $n = 3510$ QDs, SSA $n = 2778$ QDs, $p = 3.9 \times 10^{-18}$; Syn: WT $n = 932$ QDs, SSA $n = 735$ QDs, $p = 3.1 \times 10^{-4}$. **E**, Quantification of $\alpha 2$ GABA $_A$ R dwell time DT at synaptic sites in neurons expressing either eGFP-WT or eGFP-SSA. Calculations were done for all QDs (total), (trapped), or (passing) QDs at inhibitory synapses. No significant differences were found between eGFP-WT and eGFP-SSA. Total: WT $n = 390$ QDs, SSA $n = 335$ QDs, $p = 0.2$; Trapped: WT $n = 229$ QDs, SSA $n = 173$ QDs, $p = 0.4$; Passing: WT $n = 161$ QDs, SSA $n = 162$ QDs, $p = 0.9$. **F**, Quantification of eGFP-SSA clusters after 8 and 48 h of 4-AP application. t0 $n = 61$ cells, 8 h $n = 52$ cells, 48 h $n = 93$ cells, 3–6 cultures. Cluster Nb: 0–8 h: $p = 0.2$, 0–48 h: $p < 0.001$; Area: 0–8 h: $p = 0.8$, 0–48 h: $p = 0.3$; intensity: 0–8 h: $p = 0.8$, 0–48 h: $p = 0.2$. **G**, Quantification of synaptic $\alpha 2$ GABA $_A$ R clusters after 8 and 48 h of 4-AP compared with mock treated control. t0 $n = 53$ cells, 8 h $n = 50$ cells, 48 h $n = 69$ cells, 3–6 cultures. Cluster Nb: 0–8 h: $p < 0.001$, 0–48 h: $p < 0.001$; Area: 0–8 h: $p = 0.002$, 0–48 h: $p = 0.09$; Intensity: 0–8 h: $p = 0.5$, 0–48 h: $p = 0.5$. **H**, Quantification of extrasynaptic $\alpha 2$ GABA $_A$ R clusters after 8 and 48 h of 4-AP compared with mock treated control. Cluster Nb: 0–8 h: $p = 0.2$, 0–48 h: $p = 0.1$; Area: 0–8 h: $p = 0.01$, 0–48 h: $p = 0.9$; Intensity: 0–8 h: $p = 0.002$, 0–48 h: $p < 0.001$. **I**, Quantification of $\alpha 2$ GABA $_A$ R diffusion coefficients in eGFP-SSA expressing cells after 8 h of 4-AP exposure. Extra: t0 $n = 787$ QDs, 4AP 8 h $n = 365$ QDs, $p = 3.6 \times 10^{-4}$. Syn: t0 $n = 212$ QDs, 8 h $n = 187$ QDs, $p = 0.4$; 5 cultures. **J**, Quantification of explored area EA of $\alpha 2$ GABA $_A$ R after 8 h of 4-AP application. Extra: t0 $n = 1869$ QDs, 8 h $n = 1092$ QDs, $p = 0.002$. Syn: t0 $n = 753$ QDs, 8 h $n = 558$ QDs, $p = 0.09$. **K**, Quantification of $\alpha 2$ GABA $_A$ R diffusion coefficients in eGFP-SSA expressing cells after 48 h of 4-AP exposure. Extra: t0 $n = 1098$ QDs, 4AP 48 h $n = 734$ QDs, $p = 0.002$. Syn: t0 $n = 287$ QDs, 48 h $n = 198$ QDs, $p = 0.2$; 5 cultures. **L**, Quantification of explored area EA of $\alpha 2$ GABA $_A$ R after 48 h of 4-AP application. Extra: t0 $n = 2169$ QDs, 48 h $n = 1500$ QDs, $p = 0.04$. Syn: t0 $n = 633$ QDs, 48 h $n = 510$ QDs, $p = 0.002$. **M**, Quantification of $\alpha 2$ GABA $_A$ R dwell time DT in neurons expressing eGFP-SSA after 8 or 48 h of 4-AP application. Calculations were done for trapped or passing QDs at inhibitory synapses. Trapped: 8 h: $n = 189$ QDs, $p = 0.3$; 48 h: $n = 166$ QDs, $p = 0.1$; Passing: 8 h: $n = 76$ QDs, $p = 0.3$; 48 h: $n = 132$ QDs, $p = 0.9$. In **B**, **E**, **F–H**, and **M**, data are presented as mean \pm SEM. **, $p < 0.01$; ***, $p \leq 0.001$ (Mann–Whitney rank sum test). In **C**, **D**, **I**, and **L**, data are presented as median values \pm 25%–75% IQR; ***, $p \leq 0.001$ (Kolmogorov–Smirnov test). In all graphs except **E**, values were normalized to the corresponding control values.

in receptor density at synapses on chronic changes in activity.

PKA and CaMKII α pathways regulate synaptic scaling at GABAergic postsynaptic sites through gephyrin phosphorylation

To identify signaling cascades that couple the gephyrin scaffold to GABA $_A$ Rs for activity-dependent synaptic recruitment, we focused on the protein kinase A (PKA) and CaMKII α pathways. NMDA receptor-dependent compensatory adaptations at the GABAergic postsynaptic sites have been reported to be facilitated by gephyrin phosphorylation at PKA and CaMKII α locations (Flores et al., 2015). We thus transfected the eGFP-S303A/S305A (SSA) mutant (insensitive to PKA- and CaMKII α -dependent phosphorylation) into our primary hippocampal neurons and treated the neurons for 8 or 48 h with 4-AP. We did not observe differences between eGFP-WT and eGFP-SSA cluster number, cluster size, and fluorescence intensity in control conditions (Fig. 5A,B). Similarly, the SSA mutant did not significantly influence the synaptic or extrasynaptic clustering of $\alpha 2$ GABA $_A$ Rs (Fig. 5B). In contrast, the SSA mutation increased the diffusion coefficient and explored area of $\alpha 2$ GABA $_A$ Rs at both extrasynaptic and synaptic sites (Fig. 5C,D). This increase in receptor mobility did not correlate with what we expected from a normal-size scaffold. However, the $\alpha 2$ GABA $_A$ Rs dwell time at inhibitory synapses did not differ between eGFP-

SSA- and eGFP-WT-transfected neurons (Fig. 5E), indicating that the increase in receptor mobility was not accompanied by a faster synaptic escape of receptors. This is consistent with a lack of effect of the SSA mutant on $\alpha 2$ GABA $_A$ Rs clustering at synapses.

The expression of the eGFP-SSA mutant was sufficient to prevent the 4-AP (8- or 48-h) induced gephyrin and $\alpha 2$ GABA $_A$ Rs cluster growth at synapses (Fig. 5A,F,G). Interestingly, 8 and 48 h after 4-AP application, extrasynaptic $\alpha 2$ cluster intensity increased in eGFP-SSA-transfected neurons (Fig. 5H). This indicated that receptor clustering at extrasynaptic sites at the 8-h treatment time point is dependent on PKA and CaMKII α phosphorylation. However, at 48 h, receptor accumulation is independent of these two pathways. Hence, an additional pathway permits GABA $_A$ R recruitment, in particular at extrasynaptic sites, after chronic changes in activity.

We also analyzed the effect of the SSA mutant on $\alpha 2$ GABA $_A$ Rs surface diffusion. Similar to wild-type gephyrin, SSA reduced diffusion coefficient and surface exploration of $\alpha 2$ GABA $_A$ Rs at extrasynaptic sites after 8 h of 4-AP (Fig. 5I,J). This effect was maintained also after 48-h treatment (Fig. 5K,L). In contrast to wild-type gephyrin, SSA mutant increased $\alpha 2$ GABA $_A$ R confinement and decreased dwell time of GABA $_A$ Rs at synapses after 48 h of 4-AP (Fig. 5K–M). The passing $\alpha 2$ GABA $_A$ Rs remained unchanged at synapses after 8 or 48 h of 4-AP (Fig. 5M). Hence, our results indicate that gephyrin scaffold reorga-

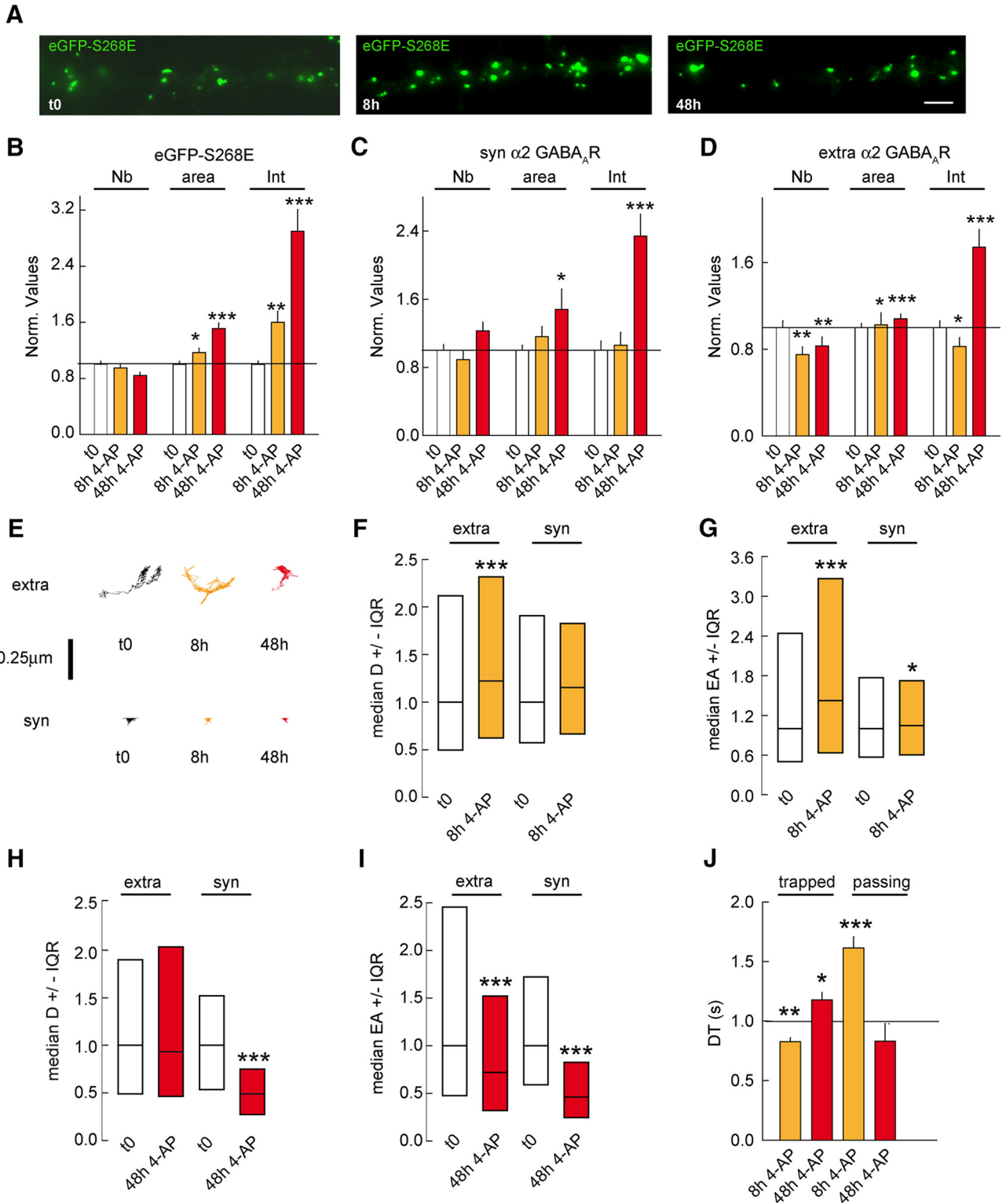


Figure 6. The ERK1/2 pathway does not influence structural synaptic adaptation. **A**, Morphologic analysis of eGFP-S268E in control (t0) or after 4-AP application for 8 or 48 h. Scale bar, 10 μ m. **B**, Quantification of eGFP-S268E clusters after 8 or 48 h of 4-AP application. t0 $n = 50$ cells, 8 h $n = 54$ cells, 48 h $n = 55$ cells, 3 cultures. Cluster Nb: 0–8 h: $p = 0.2$, 0–48 h: $p = 0.004$; Area: 0–8 h: $p = 0.02$, 0–48 h: $p < 0.001$; Intensity: 0–8 h: $p = 0.003$, 0–48 h: $p < 0.001$. 3 cultures. **C**, Quantification of synaptic $\alpha 2$ GABA_AR clusters after 8 h and 48 h of 4-AP compared with mock treated control. t0 $n = 47$ cells, 8 h $n = 50$ cells, 48 h $n = 62$ cells, 3–4 cultures. Cluster Nb: 0–8 h: $p = 0.08$, 0–48 h: $p = 0.5$; Area: 0–8 h: $p = 0.8$, 0–48 h: $p = 0.03$; Intensity: 0–8 h: $p = 0.5$, 0–48 h: $p < 0.001$. **D**, Quantification of extrasynaptic $\alpha 2$ GABA_AR clusters after 8 and 48 h of 4-AP compared with mock treated control. Cluster Nb: 0–8 h: $p = 0.006$, 0–48 h: $p = 0.007$; Area: 0–8 h: $p = 0.02$, 0–48 h: $p < 0.001$; Intensity: 0–8 h: $p = 0.04$, 0–48 h: $p < 0.001$. **E**, Example

continued

traces of $\alpha 2$ GABA_AR trajectories at extrasynaptic (extra) and synaptic (syn) sites under control condition (t0) or after 8 or 48 h of 4-AP application. Scale bar, 0.25 μ m. **F**, Quantification of $\alpha 2$ GABA_AR diffusion coefficients after 8 h of 4-AP exposure. Extra: t0 n = 1230 QDs, 4AP 8 h n = 1855 QDs, p = 3.4×10^{-6} . Syn: t0 n = 281 QDs, 8 h n = 378 QDs, p = 0.2; 3 cultures. **G**, Quantification of explored area EA of $\alpha 2$ GABA_AR after 8 h of 4-AP application. Extra: t0 n = 3402 QDs, 8 h n = 2454 QDs, p = 3.2×10^{-23} . Syn: t0 n = 843 QDs, 8 h n = 984 QDs, p = 0.02. **H**, Quantification of $\alpha 2$ GABA_AR diffusion coefficients after 48 h of 4-AP exposure. Extra: t0 n = 687 QDs, 4AP 48 h n = 1611 QDs, p = 0.4. Syn: t0 n = 73 QDs, 48 h n = 46 QDs, p = 1.6×10^{-4} . **I**, Quantification of explored area EA of $\alpha 2$ GABA_AR after 48 h of 4-AP application. Extra: t0 n = 2061 QDs, 48 h n = 546 QDs, p = 2.9×10^{-6} . Syn: t0 n = 219 QDs, 48 h n = 74 QDs, p = 6.6×10^{-7} . **J**, Quantification of $\alpha 2$ GABA_AR dwell time DT after 8 or 48 h of 4-AP application. Calculations were done for trapped or passing QDs at inhibitory synapses. Trapped: t0: n = 130 QDs, 8 h: n = 194 QDs, p = 0.007; t0: n = 85 QDs, 48 h: n = 51 QDs, p = 0.02; Passing: t0: n = 91 QDs, 8 h: n = 161 QDs, p < 0.001; t0: n = 91 QDs, 48 h: n = 31 QDs, p = 0.6. In **B–D** and **J**, data are presented as mean \pm SEM. *, $p \leq 0.05$; **, $p \leq 0.01$; ***, $p \leq 0.001$ (Mann–Whitney rank sum test). In **F–I**, data are presented as median values \pm 25%–75% IQR. *, $p \leq 0.05$; ***, $p \leq 0.001$ (Kolmogorov–Smirnov test). In all graphs, values were normalized to the corresponding control values.

nization via PKA- and CaMKII α -dependent phosphorylation at S303 and S305 is essential for GABA_AR diffusion at synapses but not at extrasynaptic sites in response to chronic changes in activity.

Synapse scaling is independent of the ERK1/2 pathway

It has been reported that gephyrin clustering is also influenced by the ERK1/2 pathway. We thus assessed whether ERK1/2 signaling influences gephyrin cluster size during chronic changes in network activity. Transgenic expression of eGFP-S268E gephyrin mutant renders gephyrin scaffold insensitive to the ERK1/2 signaling pathway (Tyagarajan et al., 2013). We therefore transfected cultured neurons with eGFP-S268E mutant and treated them with 4-AP for 8 or 48 h. Immunocytochemical analysis showed an increase in eGFP-S268E mutant cluster size after 4-AP treatment (Fig. 6A). Quantification of changes in eGFP-S268E cluster intensity confirmed an increase of 1.6- and 2.2-fold after 8 and 48 h of 4-AP treatment, respectively (Fig. 6B). This was associated with increases of 1.2- and 1.3-fold in eGFP-S268E cluster size after 8 and 48 h of 4-AP treatment (Fig. 6B). Analysis for $\alpha 2$ GABA_AR cluster intensity at synapses and at extrasynaptic sites showed a respective 2.2- and 1.8-fold increase after 48 h of 4-AP treatment, but not after 8 h (Fig. 6C,D). We conclude that the eGFP-S268E mutant is not required for the activity-dependent recruitment of gephyrin and GABA_AR within synaptic and extrasynaptic clusters. We wondered whether 4-AP induced chronic activity would impact the surface diffusion of GABA_ARs. We checked $\alpha 2$ GABA_AR diffusion coefficients after 8 or 48 h of 4-AP. Individual receptor trajectories for extrasynaptic and synaptic $\alpha 2$ GABA_AR suggested increased confinement after 48 h of enhanced activity (Fig. 6E). The $\alpha 2$ diffusion coefficients and explored area were increased by 1.2- and 1.4-fold for extrasynaptic receptors after 8 h of 4-AP (Fig. 6F,G). However, 48 h after 4-AP application, extrasynaptic receptors diffusion coefficients were unchanged (Fig. 6H), whereas QDs were more confined at extrasynaptic sites (Fig. 6I). Interestingly, 48 h of 4-AP treatment reduced synaptic $\alpha 2$ GABA_AR diffusion coefficients and explored areas at eGFP-S268E synapses (Fig. 6H,I), as observed at synapses containing eGFP-WT (Fig. 4I,J). In agreement with an increased number of $\alpha 2$ GABA_ARs at

synapses, $\alpha 2$ dwell time increased at eGFP-S268E synapses (Fig. 6J).

Therefore, we conclude that although ERK1/2 signaling is not necessary for the activity-dependent regulation of the diffusive behavior of synaptic GABA_ARs, it controls the mobility of receptors at extrasynaptic sites. These observations further confirm that synaptic and extrasynaptic receptor pools are independently regulated, and that adaptations observed at GABAergic postsynapses are independent of the ERK1/2 pathway.

GSK3 β phosphorylation of gephyrin facilitates GABA_AR diffusion after activity change

It has been reported that the GSK3 β signaling pathway postsynaptically regulates the density and size of GABAergic synapses via gephyrin phosphorylation. Pharmacological blockade of the GSK3 β pathway or expression of the S270A gephyrin mutant is sufficient to increase gephyrin cluster size (Tyagarajan et al., 2011). Hence, it is plausible that the GSK3 β pathway acts in addition to PKA and CaMKII α signaling to regulate homeostatic adaptations at GABAergic synapses. To address this question, we treated neurons transfected with eGFP-S270A gephyrin mutant with 4-AP for 8 and 48 h. Morphologic characterization showed that the GSK3 β signaling is not essential for gephyrin accumulation at synapses on chronic changes in activity (Fig. 7A,B). In contrast, the eGFP-S270A mutant fully abolished the synaptic and extrasynaptic increase in $\alpha 2$ GABA_AR clustering after 48 h of 4-AP application (Fig. 7C,D). After 8 h of 4-AP treatment, extrasynaptic $\alpha 2$ GABA_AR cluster density, size, and intensity were respectively reduced by 1.4-, 1.2-, and 1.4-fold in eGFP-S270A-expressing cells (Fig. 7D). These results implicate the GSK3 β pathway in the regulation of activity-induced GABA_AR clustering at both synaptic and extrasynaptic sites.

If the GSK3 β signaling is important for GABA_ARs accumulation at synapses in response to chronic changes in activity, then eGFP-S270A mutant expression should have no impact on $\alpha 2$ diffusion rates. However, 8 h after 4-AP application, $\alpha 2$ diffusion coefficients and explored areas were reduced by 1.3- and 1.1-fold at synaptic sites (Fig. 7E–G). This increased confinement was counterbalanced by a decrease in the time trapped receptors spent at synapses (Fig. 7J), explaining why $\alpha 2$ clustering was

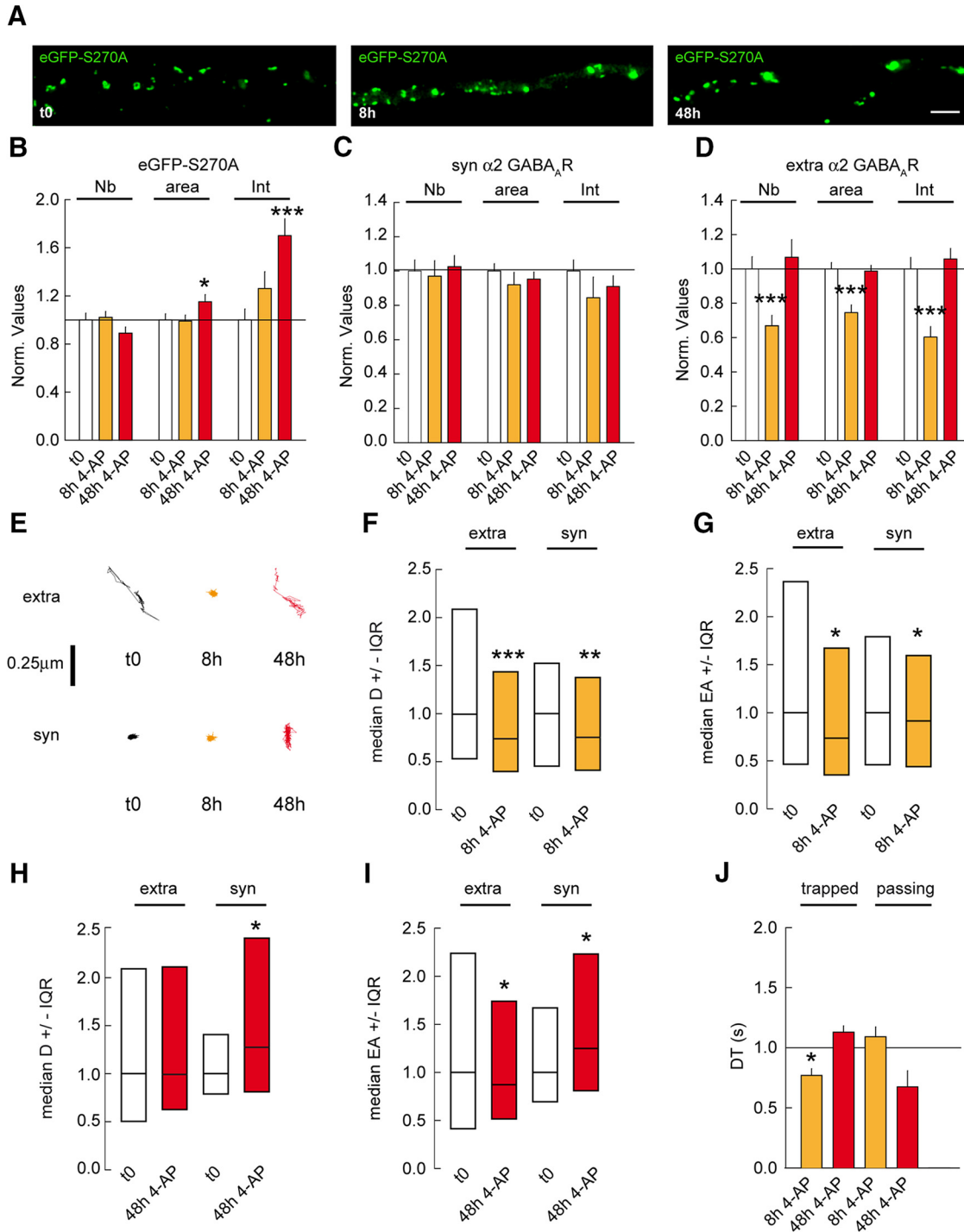


Figure 7. GSK3 β pathway influences gephyrin scaffold and GABA_ARs after changes in chronic activity. **A**, Morphology of neuron transfected with eGFP-S270A under control condition (t0) or in the presence of 4-AP after 8 or 48 h. Scale bar, 10 μ m. **B**, Quantification of eGFP-S270A clusters after 8 or 48 h of 4-AP application. t0 $n = 43$ cells, 8 h $n = 50$ cells; 48 h $n = 50$ cells, 3 cultures. Cluster Nb: 0–8 h: $p = 0.8$, 0–48 h: $p = 0.14$; Area: 0–8 h: Mann-Whitney test $p = 0.7$, 0–48 h: $p = 0.04$; Intensity: 0–8 h: $p = 0.12$, 0–48 h: $p < 0.001$. **C**, Quantification of synaptic $\alpha 2$ GABA_AR clusters after 8 and 48 h of 4-AP compared with mock treated control. t0 $n = 40$ cells, 8 h $n = 47$ cells; t0: $n = 59$ cells, 48 h $n = 52$ cells, 3–5 cultures. Cluster Nb: 0–8 h: $p = 0.8$, 0–48 h: $p = 0.7$; Area: 0–8 h: $p = 0.14$, 0–48 h: $p = 0.6$; Intensity: 0–8 h: $p = 0.03$, 0–48 h: $p = 0.4$. **D**, Quantification of extrasynaptic $\alpha 2$ GABA_AR clusters after 8 and 48 h of 4-AP compared with mock treated control. Cluster Nb: 0–8 h: $p < 0.001$, 0–48 h: $p = 0.7$; Area: 0–8 h: $p < 0.001$, 0–48 h: $p = 0.7$; Intensity: 0–8 h: $p < 0.001$, 0–48 h: $p = 0.3$. **E**, Example traces of $\alpha 2$ GABA_AR trajectories at extrasynaptic (extra) and synaptic (syn) sites under control conditions (t0) or after 8 or 48 h of 4-AP application. Scale bar, 0.25 μ m. **F**, Quantification of $\alpha 2$ GABA_AR diffusion coefficients after 8 h of 4-AP exposure. Extra: t0 $n = 1580$ QDs, 4AP 8 h $n = 1892$ QDs, $p = 1.4 \times 10^{-13}$. Syn: t0 $n = 229$ QDs, 8 h $n = 307$ QDs, $p = 8.8 \times 10^{-3}$; 3 cultures. **G**, Quantification of explored area EA of $\alpha 2$ GABA_AR after 8 h of 4-AP

continued

application. Extra: t_0 $n = 4575$ QDs, 8 h $n = 4041$ QDs, $p = 0.02$. Syn: t_0 $n = 687$ QDs, 8 h $n = 663$ QDs, $p = 0.04$. **H**, Quantification of $\alpha 2$ GABA_AR diffusion coefficients after 48 h of 4-AP exposure. Extra: t_0 $n = 314$ QDs, 4AP 48 h $n = 338$ QDs, $p = 0.05$. Syn: t_0 $n = 46$ QDs, 48 h $n = 51$ QDs, $p = 0.04$. 3 cultures. **I**, Quantification of explored area EA of $\alpha 2$ GABA_AR after 48 h of 4-AP application. Extra: t_0 $n = 939$ QDs, 48 h $n = 771$ QDs, $p = 0.02$. Syn: t_0 $n = 138$ QDs, 48 h $n = 153$ QDs, $p = 0.04$. **J**, Quantification of $\alpha 2$ GABA_AR dwell time DT after 8 or 48 h of 4-AP application. Calculations were done for trapped or passing QDs at inhibitory synapses. Trapped: t_0 : $n = 82$ QDs, 8 h: $n = 97$ QDs, $p = 0.04$; t_0 : $n = 191$ QDs, 48 h: $n = 45$ QDs, $p = 0.5$; Passing: t_0 : $n = 104$ QDs, 8 h: $n = 131$ QDs, $p = 0.5$; t_0 : $n = 211$ QDs, 48 h: $n = 23$ QDs, $p = 0.1$. In **B–D** and **J**, data are presented as mean \pm SEM. *, $p \leq 0.05$; ***, $p \leq 0.001$ (Mann–Whitney rank sum test). In **F–I**, data are presented as median values \pm 25%–75% IQR. *, $p \leq 0.05$; **, $p \leq 0.01$; ***, $p \leq 0.001$ (Kolmogorov–Smirnov test). In all graphs, values were normalized to the corresponding control values.

unchanged at synapses after 8 h of 4-AP application. On the other hand, 48 h of 4-AP application increased $\alpha 2$ diffusion coefficients by 1.3-fold as well as explored areas at synaptic sites (Fig. 7E,H,I). This was, however, not accompanied by a change in synaptic receptor dwell time (Fig. 7J). The reduction of extrasynaptic $\alpha 2$ clustering coincided with a 1.3-fold reduced explored area in eGFP-S270A-expressing cells after 8 h of 4-AP (Fig. 7E–G). Nevertheless, 48 h after 4-AP application, $\alpha 2$ diffusion coefficients and explored areas returned to baseline levels at extrasynaptic sites (Fig. 7H,I). These observations are consistent with the receptor clustering returning to control levels at extrasynaptic sites after 48 h of 4-AP (Fig. 7D). Altogether, these results show that GSK3 β signaling in addition to PKA and CaMKII α pathways tune GABA_ARs at synapses in response to chronic changes in activity.

Impairment of PKA, CAMKII α , and GSK3 β phosphorylation of gephyrin abolishes the activity-dependent regulation of GABA_ARs mobility

The analysis of the SSA and S270A mutants indicated that PKA, CAMKII α , and GSK3 β phosphorylation of gephyrin have complementary effects on gephyrin and $\alpha 2$ GABA_ARs clustering in conditions of synaptic plasticity. To show it more directly, we generated eGFP-SSA/S270A mutant, expressed it in hippocampal neurons, and treated the neurons for 8 or 48 h with 4-AP.

We found that overexpressing eGFP-SSA/S270A increased eGFP cluster size and intensity (Fig. 8A). The gephyrin cluster growth was, however, not accompanied by synaptic recruitment of $\alpha 2$ GABA_ARs (Fig. 8A). Although the density of $\alpha 2$ GABA_ARs clusters was reduced in eGFP-SSA/S270A-transfected cells, there was no major impact of the mutant on $\alpha 2$ GABA_ARs cluster size and intensity at synaptic and extrasynaptic sites (Fig. 8A).

We then characterized $\alpha 2$ GABA_AR diffusion in SSA/S270A-transfected neurons. Diffusion coefficients showed a 1.4-fold increase for extrasynaptic receptors and no significant change for synaptic receptors (Fig. 8B). This effect was consistent with the observation that $\alpha 2$ GABA_AR spent the same time at eGFP-SSA/S270A and eGFP-WT synapses (Fig. 8C). Therefore the eGFP-SSA/S270A mutant can recapitulate many of the observed phenotypes seen with SSA or S270A individual mutations.

We then characterized how chronic activity affects eGFP-SSA/S270A mutant behavior. Although the extrasynaptic GABA_ARs cluster density increased after 48 h of 4-AP in eGFP-SSA/S270A transfected cells, the triple mutant prevented the synaptic increase in gephyrin and

GABA_ARs cluster size and intensity in response to 4-AP treatment (Fig. 8D–F). The diffusion coefficient and explored area of $\alpha 2$ GABA_ARs showed no change after 8 or 48 h of 4-AP application (Fig. 8G–J). There was also no impact on receptor dwell time at synapses after chronic changes in activity (Fig. 8K).

Our results uncover a role for several signaling pathways in chronic activity-dependent modulation of gephyrin clustering and GABA_ARs surface diffusion at synapses. Our data also show that distinct signaling pathways regulate synaptic and extrasynaptic receptor clustering. Together, these results identify a novel role of GSK3 β signaling in the regulation of extrasynaptic receptor surface trafficking and GSK3 β , PKA, and CaMKII α pathways in facilitating adaptations of synaptic receptors.

Discussion

In the current study, we investigate the molecular basis for gephyrin scaffold-induced GABA_AR membrane dynamics. We identify a novel role for gephyrin posttranslational modification involving phosphorylation and dephosphorylation in regulating GABA_AR lateral diffusion. By tracking $\alpha 2$ GABA_ARs within and outside synaptic sites using QD-SPT, we demonstrate that gephyrin phosphorylation by ERK1/2 at S268, and inhibition of GSK3 β phosphorylation on gephyrin at S270, while exhibiting opposite effects on synaptic morphology, similarly influence GABA_AR diffusion properties. We analyze gephyrin scaffold organization at the nanoscale level using PALM and uncover that phosphorylation also controls gephyrin molecule packing.

Over the past decade, several independent studies have documented changes in lateral diffusion of GABA_ARs after pharmacological alteration of neuronal function within a time scale of minutes to a few hours (Lévi et al., 2008; Bannai et al., 2009; Niwa et al., 2012; Petrini et al., 2014). 4-AP application within minutes induces NMDA receptor-mediated calcium influx and calcineurin activation, leading to dephosphorylation of the GABA_AR $\gamma 2$ subunit S327 residue (Wang et al., 2003). In this context, an increase in GABA_AR diffusion constraint results from receptor dephosphorylation, whereas gephyrin scaffold loss is a secondary effect in response to receptor dispersal (Niwa et al., 2012). We identify gephyrin phosphorylation as an essential facilitator of GABA_AR diffusion dynamics in response to chronic changes in activity. More specifically, we identify a central role for PKA and CaMKII α pathways along with GSK3 β signaling in phosphorylating gephyrin to regulate activity-dependent inhibitory synapse remodeling.

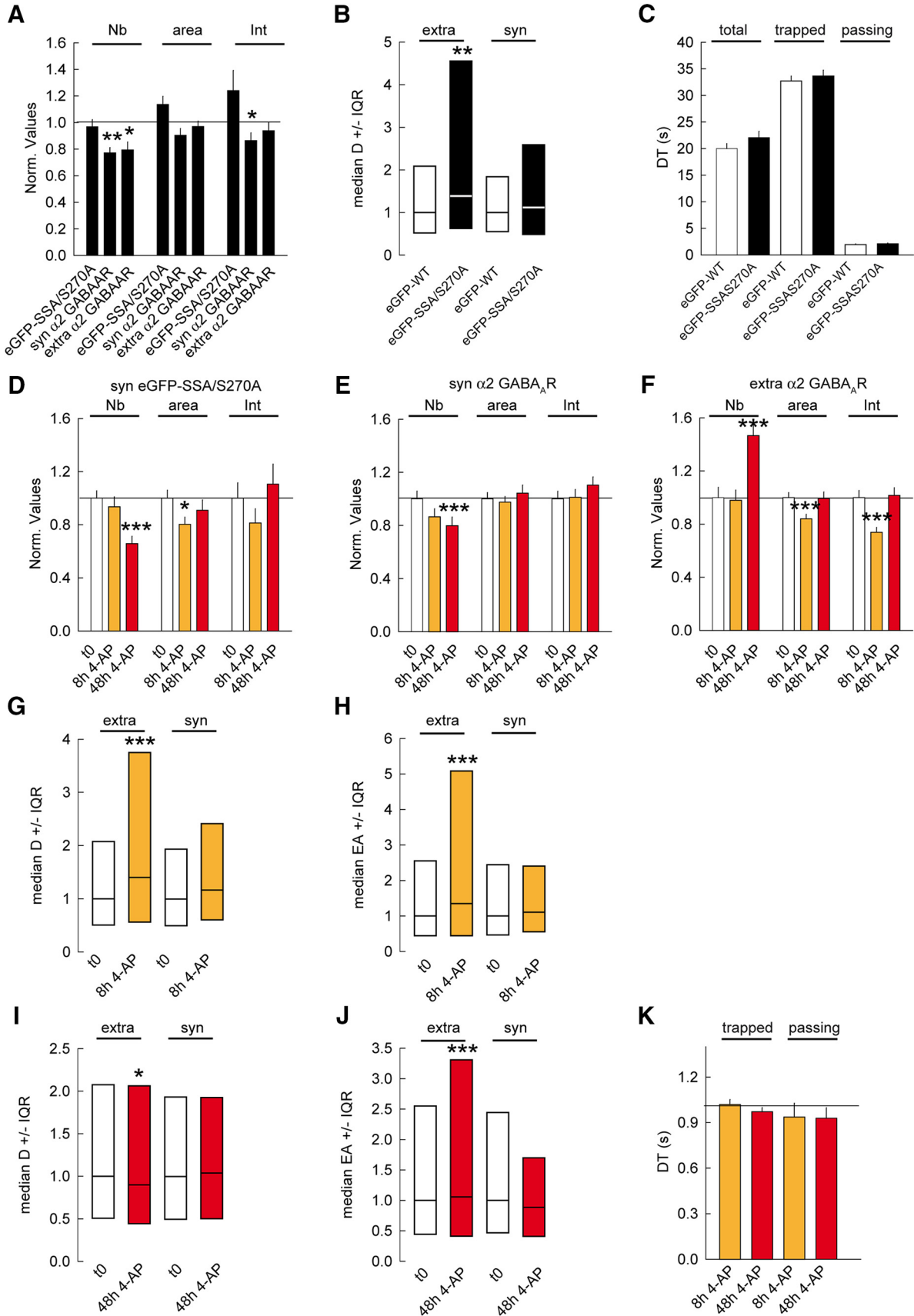


Figure 8. PKA, CAMKII α , and GSK3 β pathways are required to tune the inhibitory synapse. **A**, Quantifications of synaptic eGFP-SSA/S270 clusters and synaptic ($\alpha 2$ syn) and extrasynaptic ($\alpha 2$ extra) $\alpha 2$ GABA_AR clusters in relation to eGFP-WT show minor

continued

impact of the mutant under control condition. eGFP-WT $n = 58$ cells, eGFP-SSA/S270A $n = 62$ cells, 3 cultures. eGFP-SSA: Cluster Nb: $p = 0.6$; Area: $p = 0.1$; Intensity: $p = 0.7$. $\alpha 2$ syn: Cluster Nb: $p = 0.001$; Area: $p = 0.1$; Intensity: $p = 0.02$. $\alpha 2$ extra: Cluster Nb: $p = 0.03$; Area: $p = 0.5$; Intensity: $p = 0.2$. **B**, Quantification of median diffusion coefficient D of $\alpha 2$ GABA_AR in neurons expressing eGFP-WT or eGFP-SSA/S270A under control condition. Extra: WT $n = 823$ QDs, SSA/S270A $n = 786$ QDs, $p = 0.004$; Syn: WT $n = 261$ QDs, SSA/S270A $n = 211$ QDs, $p = 0.3$, 2 cultures. **C**, Quantification of $\alpha 2$ GABA_AR dwell time DT at synaptic sites in neurons expressing either eGFP-WT or eGFP-SSA/S270A. Calculations were done for all QDs (total), (trapped), or (passing) QDs at inhibitory synapses. No significant differences were found between eGFP-WT and eGFP-SSA/S270A. Total: WT $n = 165$ QDs, SSA/S270A $n = 183$ QDs, $p = 0.1$; Trapped: WT $n = 95$ QDs, SSA/S270A $n = 116$ QDs, $p = 0.5$; Passing: WT $n = 70$ QDs, SSA/S270A $n = 67$ QDs, $p = 0.2$. **D**, Quantification of eGFP-SSA/S270A clusters after 8 or 48 h of 4-AP application. t_0 $n = 53$ cells, 8 h $n = 45$ cells, 48 h $n = 51$ cells, 3 cultures. Cluster Nb: 0–8 h: $p = 0.3$, 0–48 h: $p < 0.001$; Area: 0–8 h: $p = 0.03$, 0–48 h: $p = 0.2$; Intensity: 0–8 h: $p = 0.3$, 0–48 h: $p = 0.9$. **E**, Quantification of synaptic $\alpha 2$ GABA_AR clusters after 8 and 48 h of 4-AP compared with mock treated control. t_0 $n = 49$ cells, 8 h $n = 49$ cells, 48 h $n = 39$ cells, 3 cultures. Cluster Nb: 0–8 h: $p = 0.2$, 0–48 h: $p < 0.001$; Area: 0–8 h: $p = 0.8$, 0–48 h: $p = 0.6$; Intensity: 0–8 h: $p = 0.2$, 0–48 h: $p = 0.9$. **F**, Quantification of extrasynaptic $\alpha 2$ GABA_AR clusters after 8 and 48 h of 4-AP compared with mock treated control. Cluster Nb: 0–8 h: $p = 0.8$, 0–48 h: $p = 0.001$; Area: 0–8 h: $p < 0.001$, 0–48 h: $p = 0.7$; Intensity: 0–8 h: $p = 0.8$, 0–48 h: $p = 0.8$. **G**, Quantification of $\alpha 2$ GABA_AR diffusion coefficients after 8 h of 4-AP exposure. Extra: t_0 $n = 624$ QDs, 4AP 8 h $n = 421$ QDs, $p = 5.4 \times 10^{-7}$. Syn: t_0 $n = 252$ QDs, 8 h $n = 173$ QDs, $p = 0.2$, 2 cultures. **H**, Quantification of explored area EA of $\alpha 2$ GABA_AR after 8 h of 4-AP application. Extra: t_0 $n = 1869$ QDs, 8 h $n = 1092$ QDs, $p = 7.8 \times 10^{-14}$. Syn: t_0 $n = 753$ QDs, 8 h $n = 516$ QDs, $p = 0.07$. **I**, Quantification of $\alpha 2$ GABA_AR diffusion coefficients after 48 h of 4-AP exposure. Extra: t_0 $n = 624$ QDs, 4AP 48 h $n = 631$ QDs, $p = 0.04$. Syn: t_0 $n = 252$ QDs, 48 h $n = 251$ QDs, $p = 0.8$. 2 cultures. **J**, Quantification of explored area EA of $\alpha 2$ GABA_AR after 48 h of 4-AP application. Extra: t_0 $n = 1092$ QDs, 48 h $n = 1890$ QDs, $p = 1.5 \times 10^{-6}$. Syn: t_0 $n = 558$ QDs, 48 h $n = 750$ QDs, $p = 0.3$. **K**, Quantification of $\alpha 2$ GABA_AR dwell time DT after 8 or 48 h of 4-AP application. Calculations were done for trapped or passing QDs at inhibitory synapses. Trapped: t_0 : $n = 116$ QDs, 8 h: $n = 84$ QDs, 48 h: $n = 43$ QDs, 0–8 h: $p = 0.2$; 0–48 h: $p = 0.02$; Passing: t_0 : $n = 67$ QDs, 8 h: $n = 46$ QDs, 48 h: $n = 43$ QDs, 0–8 h: $p = 0.2$; 0–48 h: $p = 0.1$. In **A**, **C–F**, and **K**, data are presented as mean \pm SEM. *, $p \leq 0.05$; ***, $p \leq 0.001$ (Mann–Whitney rank sum test). In **G–J**, data are presented as median values \pm 25%–75% IQR. *, $p \leq 0.05$; ***, $p \leq 0.001$ (Kolmogorov–Smirnov test). In all graphs except **C**, values were normalized to the corresponding control values.

Structure of the gephyrin scaffold requires phosphoregulation of gephyrin molecules

At GABAergic synapses, the role of phosphorylation for gephyrin scaffold compaction has yet to be reported. The fluorescence microscopy data (Fig. 1B) inform us about average area and intensity per cluster. PALM microscopy informs us about the actual density of molecules per surface area (Fig. 3). The number of molecules per synapse using PALM imaging can be roughly estimated by multiplying the mean surface area of the cluster by the density of gephyrin molecules per surface unit. Values of ~212, 156, and 220 were found for the gephyrin WT, S268E, and S270A respectively. Interestingly, these estimations are consistent with the measurements of the mean cluster fluorescence intensity for the S268E and S270A mutants.

The hexameric gephyrin lattice model was proposed based on G and E domain crystal structures available at the time. However, in recent years, atomic force microscopy (AFM) and small-angle X-ray scattering (SAXS) structure of full-length gephyrin has shown that gephyrin only exists as trimers, as individual E domains are in an open extended confirmation (Sander et al., 2013). Pennacchietti et al. (2017) have shown that after iLTP, gephyrin reorganizes itself into distinct subsynaptic nanodomains. Full-length gephyrin can exist in open or closed confirmations based on the linker domain folding (Sander et al., 2013). All the gephyrin phosphorylation sites have been mapped to the linker domain, suggesting that phosphorylation is a strong candidate for determining open and closed states within gephyrin nanodomains. This could in turn determine the distance between two nanodomains and/or total number of nanodomains within a given synapse.

Gephyrin-independent GABA_AR adaptations at synaptic sites

It has long been assumed that alterations in GABA_AR and/or gephyrin cluster intensity are indicative of the number of molecules found at the synapse, and thereby a direct correlate for changes in synapse structure and function. Here we report that disrupting gephyrin scaffold via the expression of the eGFP-DN mutant does not increase the diffusion properties of GABA_ARs at synaptic sites. This observation was unexpected, as loss of the scaffolding apparatus should have increased receptor diffusion also at synaptic sites. It has been reported that eGFP-DN expression significantly reduces mIPSC amplitude and frequency, without leading to a complete loss of GABAergic synaptic transmission (Ghosh et al., 2016). Our observation suggests that a pool of gephyrin-independent GABA_ARs are present in neurons. Recently, the GIT1/ β PIX/Rac1/PAK signaling pathway was shown to contribute to GABAergic transmission. β PIX is a guanine nucleotide exchange factor (GEF) for Rac1 activating PAK and contributes to GABA_AR stability (Smith et al., 2014). Similar signaling mechanisms could be operational even in the absence of gephyrin scaffold to maintain the membrane pool of GABA_ARs.

Independent behavior of GABA_ARs at synaptic and extrasynaptic sites

Postsynaptic receptor trapping is adaptable depending on phosphorylation events that impinge on scaffold–scaffold or receptor–scaffold interactions (Choquet and Triller, 2013). It became clear with the development of SPT approaches that receptors are also hindered in their diffusion outside synapses via molecular crowding but also through specific protein–protein interactions. A receptor–

gephyrin interaction outside inhibitory synapses has been reported earlier (Ehrensperger et al., 2007). GABA_ARs also colocalize and interact with clathrin-enriched endocytic zones (EZs) that are mostly localized extrasynaptically (Smith et al., 2012). Receptors in EZs do not necessarily undergo internalization. They can be part of a reserve pool of receptors rapidly available upon increase in synaptic activity (Petrini et al., 2014). Conversely, the GABA_AR-AP2 interaction within EZs has been shown to indirectly control receptor mobility and number at synapses (Smith et al., 2012).

However, our data show independent behavior of GABA_ARs at synaptic and extrasynaptic sites. After 8 h of 4-AP treatment, α 2 GABA_ARs were confined at extrasynaptic sites without influencing the diffusion property of synaptic receptors. In contrast, after 48 h of 4-AP treatment, α 2 GABA_AR confinement at extrasynaptic sites was ceased, and this was followed by an increase in receptor confinement at synapses, suggesting that GABA_AR retention at extrasynaptic sites prevents their synaptic capture/accumulation. However, after 8 h of 4-AP treatment, neurons expressing eGFP-S268E mutant show a reduction in receptor confinement at extrasynaptic locations, without affecting synaptic receptor diffusion. Therefore, removing diffusion constraints onto extrasynaptic GABA_ARs does not facilitate receptor recruitment at synapses. In addition, after 8 h of 4-AP treatment, neurons expressing eGFP-S270A mutant show increased confinement of GABA_ARs at both extrasynaptic and synaptic locations, indicating that confining GABA_ARs at extrasynaptic locations does not prevent diffusion-capture of receptors.

Synaptic adaptation is facilitated by gephyrin phosphorylation

We present evidence for a biphasic model for activity-dependent plasticity at GABAergic postsynapse. Acute 4-AP treatment increases and chronic 4-AP treatment decreases α 2 GABA_AR lateral diffusion. The observed increase in GABA_AR diffusion after acute 4-AP treatment can be explained by an increase in synaptic escape of receptors, leading to reduced postsynaptic clustering and dispersal of gephyrin molecules away from the synapse (Bannai et al., 2009). On the contrary, we show here that chronic 4-AP treatment leads to synaptic immobilization and recruitment of GABA_AR α 2 and gephyrin. These discrepancies are probably due to the distinct signaling pathways activated by the acute and chronic changes in activity. Short-term 4-AP application induces NMDAR-mediated calcium influx and calcineurin activation, leading to dephosphorylation of GABA_AR γ 2 subunit S327 residue (Bannai et al., 2009). In this context, the relief in GABA_AR diffusion constraints arises from receptor dephosphorylation, whereas gephyrin loss is a consequence of receptor dispersal (Niwa et al., 2012). In contrast, we show that chronic changes in activity affect first the recruitment of gephyrin at synapses, and then allow the recruitment of GABA_ARs. PKA and CaMKII α signaling act downstream of NMDA receptor to facilitate compensatory postsynaptic adaptations at GABAergic synapses (Flores et al., 2015). Our data extends this understanding by

demonstrating a role for the GSK3 β pathway in addition to PKA and CaMKII α pathways in facilitating gephyrin scaffold organization of individual GABA_ARs after prolonged changes in activity.

References

- Bannai H, Lévi S, Schweizer C, Inoue T, Launey T, Racine V, Sibarita J-B, Mikoshiba K, Triller A (2009) Activity-dependent tuning of inhibitory neurotransmission based on GABAAR diffusion dynamics. *Neuron* 62:670–682. [CrossRef Medline](#)
- Bannai H, Niwa F, Sherwood MW, Shrivastava AN, Arizono M, Miyamoto A, Sugiura K, Lévi S, Triller A, Mikoshiba K (2015) Bidirectional control of synaptic GABAAR clustering by glutamate and calcium. *Cell Rep* 13:2768–2780. [CrossRef Medline](#)
- Bats C, Groc L, Choquet D (2007) The interaction between Stargazin and PSD-95 regulates AMPA receptor surface trafficking. *Neuron* 53:719–734. [CrossRef Medline](#)
- Chamma I, Heubl M, Chevy Q, Renner M, Moutkine I, Eugène E, Poncer JC, Lévi S (2013) Activity-dependent regulation of the K/Cl transporter KCC2 membrane diffusion, clustering, and function in hippocampal neurons. *J Neurosci* 33:15488–15503. [CrossRef](#)
- Charrier C, Machado P, Tweedie-Cullen RY, Rutishauser D, Mansuy IM, Triller A (2010) A crosstalk between β 1 and β 3 integrins controls glycine receptor and gephyrin trafficking at synapses. *Nat Neurosci* 13:1388–1395. [CrossRef Medline](#)
- Chen JL, Villa KL, Cha JW, So PTC, Kubota Y, Nedivi E (2012) Clustered dynamics of inhibitory synapses and dendritic spines in the adult neocortex. *Neuron* 74:361–373. [CrossRef Medline](#)
- Choquet D, Triller A (2013) The dynamic synapse. *Neuron* 80:691–703. [CrossRef Medline](#)
- Ehrensperger M-V, Hanus C, Vannier C, Triller A, Dahan M (2007) Multiple association states between glycine receptors and gephyrin identified by SPT analysis. *Biophys J* 92:3706–3718. [CrossRef Medline](#)
- Flores CE, Nikonenko I, Mendez P, Fritschy J-M, Tyagarajan SK, Muller D (2015) Activity-dependent inhibitory synapse remodeling through gephyrin phosphorylation. *Proc Natl Acad Sci USA* 112:E65–E72. [CrossRef](#)
- Ghosh H, Auguadri L, Battaglia S, Simone Thirouin Z, Zemoura K, Messner S, Acuña MA, Wildner H, Yévenes GE, Dieter A, Kawasaki H, O Hottiger M, Zeilhofer HU, Fritschy J-M, Tyagarajan SK (2016) Several posttranslational modifications act in concert to regulate gephyrin scaffolding and GABAergic transmission. *Nat Commun* 7:13365. [CrossRef Medline](#)
- Lardi-Studler B, Smolinsky B, Petitjean CM, Koenig F, Sidler C, Meier JC, Fritschy JM, Schwarz G (2007) Vertebrate-specific sequences in the gephyrin E-domain regulate cytosolic aggregation and postsynaptic clustering. *J Cell Sci* 120:1371–1382. [CrossRef Medline](#)
- Lévi S, Schweizer C, Bannai H, Pascual O, Charrier C, Triller A (2008) Homeostatic regulation of synaptic GlyR numbers driven by lateral diffusion. *Neuron* 59:261–273. [CrossRef Medline](#)
- Lüscher B, Fuchs T, Kilpatrick CL (2011) GABAA receptor trafficking-mediated plasticity of inhibitory synapses. *Neuron* 70:385–409. [CrossRef Medline](#)
- Muir J, Arancibia-Carcamo IL, MacAskill AF, Smith KR, Griffin LD, Kittler JT (2010) NMDA receptors regulate GABAA receptor lateral mobility and clustering at inhibitory synapses through serine 327 on the γ 2 subunit. *Proc Natl Acad Sci USA* 107:16679–16684. [CrossRef](#)
- Niwa F, Bannai H, Arizono M, Fukatsu K, Triller A, Mikoshiba K (2012) Gephyrin-independent GABA(A)R mobility and clustering during plasticity. *PLoS ONE* 7:e36148. [CrossRef Medline](#)
- Pennacchiotti F, Vascon S, Nieuws T, Rosillo C, Das S, Tyagarajan SK, Diaspro A, Del Bue A, Petrini EM, Barberis A, Cella Zanacchi F (2017) Nanoscale molecular reorganization of the inhibitory postsynaptic density is a determinant of GABAergic synaptic potentiation. *J Neurosci* 37:1747–1756. [CrossRef Medline](#)

- Petrini EM, Barberis A (2014) Diffusion dynamics of synaptic molecules during inhibitory postsynaptic plasticity. *Front Cell Neurosci* 8:300. [CrossRef](#) [Medline](#)
- Petrini EM, Ravasenga T, Hausrat TJ, Iurilli G, Olcese U, Racine V, Sibarita J-B, Jacob TC, Moss SJ, Benfenati F, Medini P, Kneussel M, Barberis A (2014) Synaptic recruitment of gephyrin regulates surface GABAA receptor dynamics for the expression of inhibitory LTP. *Nat Commun* 5:3921. [CrossRef](#)
- Rannals MD, Kapur J (2011) Homeostatic strengthening of inhibitory synapses is mediated by the accumulation of GABA(A) receptors. *J Neurosci* 31:17701–17712. [CrossRef](#) [Medline](#)
- Renner M, Schweizer C, Bannai H, Triller A, Lévi S (2012) Diffusion barriers constrain receptors at synapses. *PLoS ONE* 7:e43032. [CrossRef](#)
- Saliba RS, Michels G, Jacob TC, Pangalos MN, Moss SJ (2007) Activity-dependent ubiquitination of GABA(A) receptors regulates their accumulation at synaptic sites. *J Neurosci* 27:13341–13351. [CrossRef](#)
- Sander B, Tria G, Shkumatov AV, Kim EY, Grossmann JG, Tessmer I, Svergun DI, Schindelin H (2013) Structural characterization of gephyrin by AFM and SAXS reveals a mixture of compact and extended states. *Acta Crystallogr D Biol Crystallogr* 69:2050–2060. [CrossRef](#) [Medline](#)
- Smith KR, Davenport EC, Wei J, Li X, Pathania M, Vaccaro V, Yan Z, Kittler JT (2014) GIT1 and β PIX are essential for GABA(A) receptor synaptic stability and inhibitory neurotransmission. *Cell Rep* 9:298–310. [CrossRef](#) [Medline](#)
- Smith KR, Muir J, Rao Y, Browarski M, Gruenig MC, Sheehan DF, Haucke V, Kittler JT (2012) Stabilization of GABA(A) receptors at endocytic zones is mediated by an AP2 binding motif within the GABA(A) receptor β 3 subunit. *J Neurosci* 32:2485–2498. [CrossRef](#) [Medline](#)
- Specht CG, Izeddin I, Rodriguez PC, Beheiry El M, Rostaing P, Darzacq X, Dahan M, Triller A (2013) Quantitative nanoscopy of inhibitory synapses: counting gephyrin molecules and receptor binding sites. *Neuron* 79:308–321. [CrossRef](#)
- Tyagarajan SK, Ghosh H, Yévenes GE, Imanishi SY, Zeilhofer HU, Gerrits B, Fritschy J-M (2013) Extracellular signal-regulated kinase and glycogen synthase kinase β regulate gephyrin postsynaptic aggregation and GABAergic synaptic function in a calpain-dependent mechanism. *J Biol Chem* 288:9634–9647. [CrossRef](#)
- Tyagarajan SK, Ghosh H, Yévenes GE, Nikonenko I, Ebeling C, Schwerdel C, Sidler C, Zeilhofer HU, Gerrits B, Müller D, Fritschy J-M (2011) Regulation of GABAergic synapse formation and plasticity by GSK3 β -dependent phosphorylation of gephyrin. *Proc Natl Acad Sci USA* 108:379–384. [CrossRef](#)
- van Versendaal D, Rajendran R, Saiepour MH, Klooster J, Smit-Rigter L, Sommeijer J-P, De Zeeuw CI, Hofer SB, Heimel JA, Levelt CN (2012) Elimination of inhibitory synapses is a major component of adult ocular dominance plasticity. *Neuron* 74:374–383. [Cross-Ref](#) [Medline](#)
- Villa KL, Berry KP, Subramanian J, Cha JW, Oh WC, Kwon H-B, Kubota Y, So PTC, Nedivi E (2016) Inhibitory synapses are repeatedly assembled and removed at persistent sites in vivo. *Neuron* 89:756–769. [CrossRef](#)
- Vlachos A, Reddy-Alla S, Papadopoulos T, Deller T, Betz H (2013) Homeostatic regulation of gephyrin scaffolds and synaptic strength at mature hippocampal GABAergic postsynapses. *Cereb Cortex* 23:2700–2711. [CrossRef](#) [Medline](#)
- Wang J, Liu S, Haditsch U, Tu W, Cochrane K, Ahmadian G, Tran L, Paw J, Wang Y, Mansuy I, Salter MM, Lu YM (2003) Interaction of calcineurin and type-A GABA receptor gamma 2 subunits produces long-term depression at CA1 inhibitory synapses. *J Neurosci* 23:826–836. [Medline](#)
- Yu W, Jiang M, Miralles CP, Li R-W, Chen G, De Blas AL (2007) Gephyrin clustering is required for the stability of GABAergic synapses. *Mol Cell Neurosci* 36:484–500. [CrossRef](#) [Medline](#)